ECC-SMART PROJECT

Joint European Canadian Chinese development of Small Modular Reactor Technology

Grant Agreement Number: 945234

H2020 – NFRP-2019-2020

Start Date of the Project: 1/09/2020

Duration: 54 Months

Deliverable Title:	**D3.4 Report on the improved system codes describing how they improved**
Lead party:	20-NPIC
Author(s):	Xuebin Zhao(NPIC), Pan Wu(XJTU),Junxiang Zhao(NPIC), Tamás Varju (BME), Armando Nava Dominguez (CNL), Yuliia Filonova (IPP), Vladislav Filonov (IPP), Walter Ambrosini (UNIPI), Andrea Pucciarelli (UNIPI)
Participant(s):	NPIC, XJTU, BME, CNL, IPP
Due Date:	30/11/2024

Version Number:

1.1

Approved by: Coordinator

Date: December 4th 2024

Dissemination level		
PU	Public	**X**
CO	Confidential: only for ECC-SMART Partners (including the Commission Services)	
EU-RES	Classified Information: RESTREINT UE*	
EU-CON	Classified Information: CONFIDENTIEL UE*	
EU-SEC	Classified Information: SECRET UE*	

**Commission Decision 2005/444/EC*

Document History – Version Control

Version	Issue Date	Stage	Description of Changes	Contributor
0.0		Draft Version	First integrated version	Xuebin Zhao(NPIC), Junxiang Zhao(NPIC), Walter Ambrosini(UniP) Ivan Otic (KIT), Tamás Varju (BME), Armando Nava Dominguez (CNL), Yuliia Filonova (IPP)
1.0	29/11/2024	Submission		Xuebin Zhao(NPIC), Junxiang Zhao(NPIC), Walter Ambrosini(UniPi) Ivan Otic (KIT), Tamás Varju (BME), Armando Nava Dominguez (CNL), Yuliia Filonova (IPP)
1.1	3/12/2024	Submission	Add Vladislav Filonov from IPP in the author list, and add some abbreviations	Xuebin Zhao (NPIC), Walter Ambrosini (UniPi), Vladislav Filonov (IPP),Yuliia Filonova (IPP)

Project information

Project acronym:	ECC-SMART
Project title:	Joint European Canadian Chinese development of Small Modular Reactor Technology

Grant Agreement n°	945234
Start date:	1.9.2020
Duration	54 months
Programme:	Framework Programme for Research and Innovation (2019-2020) under the call NFRP-2019-2020
Coordinator:	Centrum Výzkumu Řež, s.r.o. (Czech Republic)

Document information

Work package:	WP3 Thermal Hydraulics and Safety of the SCW-SMR
Contractual Date of Delivery:	30.11.2024
Actual Date of Delivery to the EC:	04.12.2024
Document type:	Report
Dissemination level:	Public (PU)
Number of pages:	68

Abstract:

This deliverable outlines the improvements achieved in the system codes used by the participants in Task 3.3 of ECC-SMART project, aiming to set up upgraded models suitable for the analyses performed in the frame of WP3. China advanced the SCTRAN code, collected data, and ensured the safety of supercritical water reactors. European teams, with tools like RELAP5, APROS, and TMM, analyzed parameter changes in supercritical water reactors. Canada's National Lab improved ASSERT-PV SC for hydraulic resistance in supercritical flows, showing better predictions post-correction.

Copyright / Disclaimer

The document is property of the ECC-SMART consortium members. This document reflects only the author's view. It does not represent the view of the European Commission and the European Commission is not responsible for any use that may be made of the information it contains. This deliverable contains original unpublished work except where clearly indicated otherwise. Acknowledgement of previously published material and of the work of others has been made through appropriate citation, quotation or both. No copying or distributing, in any form or by any means, is allowed without the prior written agreement of the owner of the property rights.

The ECC-SMART project has received funding from the Euratom research and training programme 2019-2020 under grant agreement No 945234.

Executive Summary

This deliverable describes the improvements achieved in the system codes used by the participants in Task 3.3 of ECC-SMART project, aiming to set up upgraded models suitable for the analyses performed in the frame of WP3.

The ECC-SMART project, a joint European, Canadian, and Chinese endeavor, focuses on the development of Small Modular Reactor Technology (SMRT). The main objectives of the project are to define the design requirements for the future SCW-SMR technology, to develop the pre-licensing study and guidelines for the demonstration of the safety in the further development stages of the SCW-SMR concept including the methodologies and tools to be used and to identify the key obstacles for the future SMR licensing and propose a strategy for this process. To reach these objectives, specific technical knowledge gaps were defined and were assessed to achieve the future smooth licensing and implementation of the SCW-SMR technology.

The document outlines the specific contributions made by each team involved in the project. It covers the Chinese team's efforts in enhancing system analysis codes, gathering experimental data, and conducting safety evaluations for supercritical water-cooled reactors. Additionally, it underscores the European team's involvement in the development and validation of these analysis codes, along with the Canadian team's pivotal role in advancing small modular reactor technology.

In particular, NPIC used the SCTRAN code, the University of Pisa adopted the RELAP5 code, BME the APROS code, IPP used a code based on the Transfer Matrix Method and CNL adopted the subchannel code ASSERT-PV.

Table of contents

List of acronyms and abbreviations 8
List of tables 8
List of figures 9
1 Improvements in the System Analysis Program for SCWR - China 12
1.1 Development and Verification of Constitutive Models: 12
1.2 Research on Trans-critical Processing Methods: 12
1.3 Application of the System Analysis Program in Safety Evaluation: 13
1.4 Broad Parameter Range Wall Heat Transfer Model: 13
1.5 Improvement of Critical Heat Flux Model: 13
1.6 Optimization of Resistance Coefficient Model: 13
1.7 Enhancement of Heat Transfer Models: 13
1.8 Development of Radiation Heat Transfer Model: 13
1.9 Optimization of SCTRAN Calculation Process: 13
1.10 Verification and Testing: 13
1.11 Application of Supercritical Water Reactor System Analysis Program 14
1.11.1 CSR1000 Safety Analysis 14
1.12 Conclusions 23
2 Customising RELAP5 for SCWR - UNIPI 24
2.1 Adopted versions of the RELAP5 code 24
2.2 Changes made to the RELAP5 code by ISS 24
2.3 Reference experimental data from IPP 26
2.4 RELAP5/MOD3.3 nodalisation and calculation procedure 28
2.5 Obtained results 29
2.6 Concluding remarks 34
3 Improvements of the APROS system code for analyses under supercritical pressure conditions - BME 35
3.1 Modelling supercritical pressure water with APROS 35
3.2 Improvement of the APROS code based on the benchmarking 36
3.3 Concluding remarks 38
4 Adaptation and improvement of Transfer Matrix Method for analyses the flows with SCP - IPP 39
4.1 Introductory remarks 39
4.2 Adaptation of TMM for analyses heat transfer regimes with extremely nonlinear behavior of thermophysical properties 40

4.2.1 General description of the accepted formalism and the concept of adaptation 40
4.2.2 Demonstration of stability of the proposed method 42
4.3 Application of the TMM method for regimes with HTD and correlation "robustness" map preparation 44
4.4 Non-linear differential method for predicting HTC and PLF 49
4.4.1 Method description 49
4.4.2 Numerical solution 50
4.4.3 Application of differential procedure for calculating regimes with HTD 53
4.5 Concluding remarks 57
5 Subchannel Analysis for Supercritical Flows - CNL 58
5.1 Subchannel code ASSERT-PV 58
5.2 Experiments 59
5.3 Concluding remarks 63
6 References: 64

List of acronyms and abbreviations

AECL	Atomic Energy of Canada Ltd
APROS	System analysis software
ASSERT-PV	System analysis software
BME	Budapesti Műszaki és Gazdaságtudományi Egyetem / Budapest University of Technology and Economics
CR	Control Rod
DLL	Dynamic Link Library
ECC-SMART	(Joint) European Canadian Chinese development of Small Modular Reactor Technology
GIF	Generation IV International Forum
IAEA	International Atomic Energy Agency
LOFA	Loss of coolant flow accident
MCST	Maximum cladding surface temperature
NPIC	Nuclear Power Institute of China
NTUU	National Technical University of Ukraine
RCP	Reactor coolant pump
RMS	Root Mean Square
RELAP-5	System analysis software
SBO	Station Blackout
SC	Supercritical
SCTRAN	System analysis software
SCW-SMR	Supercritical water-cooled small modular reactor
SCWR	Supercritical Water-Cooled Reactor
UNIPI	University of Pisa
XJTU	Xi'an Jiaotong University

List of tables

Table 1. Boundary conditions applied to the bundles during the experiments.....27

Table 2. The main operating parameters for chosen NTUU regimes 53

Table 3. The comparison of total pressure drop values 56

Table 4. Uncertainties of measured and calculated parameters 60

Table 5. Code bias and RMS in the ASSERT predictions of pressure drops 61

Table 6. Results of sensitivity analysis using NTUU tube tests 61

Table 7. Results of sensitivity analysis using NTUU 3-rod tests 62

List of figures

Figure 1. Partial loss of main coolant flow 14

Figure 2. Loss of offsite power 15

Figure 3. Sensitivity analysis of RCP delay time in loss of offsite power 15

Figure 4. Main coolant control system failure 16

Figure 5. Main steam line valve closure 17

Figure 6. Loss of feedwater heating 17

Figure 7. Uncontrolled CR withdrawal 18

Figure 8. Pump seizure 19

Figure 9. Variations of core parameters in the first 40 s of LOFA 20

Figure 10. Thermal–hydraulic response in long-term LOFA. (a) The ICS parameters. (b) The core flowrate variations. (c) The MCST evolutions of both passes 20

Figure 11. Sensitivity analysis of RMT actuation delay time in LOFA 21

Figure 12. Core depressurization. (a) System parameter variation with time. (b) The void fraction of the lower and upper plenum and the GDCS flowrate. (c) The MCST variation of both passes in 2000 s 23

Figure 13. Rod bundle configurations considered in Razumovskiy et al. (2008, 2016) 26

Figure 14. Results obtained with the ISS version of RELAP5 with Mokry and Bishop correlations for 1-rod bundle data from IPP. 30

Figure 15. Results obtained with the ISS version of RELAP5 with Mokry and Bishop correlations for 3-rod bundle data from IPP. 32

Figure 16. Results obtained with the ISS version of RELAP5 with Mokry and Bishop correlations for 7-rod bundle data from IPP. 33

Figure *17* Wall and Bulk temperature results of a bare tube case with the original and the new DLL 37

Figure *18* Wall and Bulk temperature results of a rod bundle case with the original and the new DLL 37

Figure 19. Illustration of the "basic" and "correction" values on the elementary section for the current iteration 42

Figure 20. The problem of implicit correlations unambiguousness 43

Figure 21. Results of calculations obtained by TMM in comparison to COMSOL FEM application, a – Regime #1, b – Regime #2 44

Figure 22. Calculation results by TMM for the selected cases (NTUU, 1-rod bundle) 45

Figure 23. Calculation results by TMM for the selected cases (NTUU, 3-rod bundle) 45

Figure 24. Calculation results by TMM for the selected cases (NTUU, 7-rod bundle) 46

Figure 25. Calculation results obtained for HTD cases (NTUU, 1-, 3- and 7- rod bundles) using correlations chosen based on “robustness maps” analysis 48

Figure 26. General view of the computational mesh 51

Figure 27. The scheme of coupling the 2D Differential procedure (“Narrow channel”) with the 1D TMM method 52

Figure 28. Axial distribution of bulk flow and wall temperatures for NHT regimes: a – 3R(N), b – 7R(N) 55

Figure 29. Axial distribution of bulk flow and wall temperatures for regimes with HTD: a – 3R(D), b – 7R(D) 55

Figure 30. The calculated values of turbulent viscosity obtained for each regime (reference diameters calculated according to (4-19)) 56

Abstract

The project aims to establish design specifications for future SCW-SMR tech, develop pre-licensing studies, and identify hurdles for SMR licensing, proposing strategies to overcome them. It also seeks to fill technical knowledge gaps for smooth adoption of SCW-SMR technology.

This deliverable outlines advancements in system codes for Task 3.3 of the ECC-SMART project, focusing on enhancing models for WP3 analyses.

The Nuclear Power Institute of China and Xi'an Jiaotong Uiversity from China, has enhanced system codes, the SCTRAN code, collected experimental data, and assessed supercritical water-cooled reactors' safety. They've utilized domestic facilities to gather crucial heat transfer data, aiding code improvements and optimizing models through numerical simulations.

The European teams, including University of Pisa using RELAP5, BME using APROS, and IPP using the Transfer Matrix Method (TMM), study the rapid changes in parameters such as pressure, temperature, and void fraction during the rapid supercritical accident process of supercritical water reactors, and the characteristics of the design of future SCWR.

Canada National Lab recent validation exercise has highlighted the need for a correction factor in ASSERT-PV SC to address hydraulic resistance in supercritical diabatic flows, especially near critical points. Early results show improved predictions after applying this factor. This exercise is crucial for evaluating the code's improvements.

1 Improvements in the System Analysis Program for SCWR - China

1.1 Development and Verification of Constitutive Models:

A flow and heat transfer model were developed based on experimental data and empirical correlations, covering a wide range of parameters from subcritical to supercritical regions.

The model utilizes parameters such as wall temperature, heat flux density, and pressure to determine the flow and heat transfer modes of the fluid.

Above the pseudo-critical region of 19 MPa, a more precise lookup table method is employed for calculating heat transfer coefficients, ensuring smooth transitions between different modes.

1.2 Research on Trans-critical Processing Methods:

Addressed the rapid changes in parameters such as pressure, temperature, and void fraction during the rapid trans-critical accident process of a supercritical water reactor.

Combined variable time steps and Jacobian coefficient matrix to resolve computational instability and numerical oscillation issues in the trans-critical process. Large time steps can lead to the loss of information in the coefficient matrix, while reducing the time step size is beneficial for improving the convergence properties of nonlinear systems of equations. The selection of time step size should be dynamically controlled for each computational control volume. The variable time step matrix is shown in Eq.(1-1), where Δt_1 represents the impact of the pressure change rate on matrix solving, Δt_2 represents the influence of pressure changes on the mass partial derivative for each control volume in matrix solving, Δt_3 represents the influence of pressure changes on the internal energy partial derivative for each control volume in matrix solving, and Δt_4 represents the influence of the ratio of control volume mass to mass flow rate on matrix solving. a_1, a_2, a_3, a_4 are empirical coefficients and are the Jacobian coefficient, which can be obtained through limited attempts. The strategy of dynamic time step control can be referred to RETRAN method (McFadden et al. 1988).

$$\Delta t = \min\left(\Delta t_1, \Delta t_2, \Delta t_3, \Delta t_4\right) \tag{1-1}$$

$$\Delta t_1 = a_1 \frac{P}{\frac{\partial P}{\partial U}\frac{\partial U}{\partial t} + \frac{\partial P}{\partial M}\frac{\partial M}{\partial t}} \tag{1-2}$$

$$\Delta t_2 = \frac{a_2}{\frac{\partial P}{\partial M}\frac{\partial M}{\partial t}} \tag{1-3}$$

$$\Delta t_3 = \frac{a_3}{\frac{\partial P}{\partial U}\frac{\partial U}{\partial t}} \tag{1-4}$$

$$\Delta t_4 = a_4 \frac{M}{W} \tag{1-5}$$

1.3 Application of the System Analysis Program in Safety Evaluation:

Applied the improved system analysis program to safety evaluation and system design research for supercritical water reactors.

Further refined the program's constitutive model and numerical solution methods through numerical simulation feedback, enhancing predictive accuracy.

1.4 Broad Parameter Range Wall Heat Transfer Model:

A new wide parameter range wall heat transfer model was developed, encompassing 12 heat transfer modes, including single-phase liquid to supercritical water condensation heat transfer.

1.5 Improvement of Critical Heat Flux Model:

Adopted the 2006 CHF lookup table for calculating critical heat flux, incorporating a diameter correction factor for different tube diameter calculations.

1.6 Optimization of Resistance Coefficient Model:

Enhanced the calculation methods for single-phase friction coefficients and two-phase friction coefficients to more accurately reflect the friction effects between fluids and walls.

1.7 Enhancement of Heat Transfer Models:

Improved heat transfer models, especially near the critical enthalpy value, to account for the significant property changes of water under supercritical pressure.

1.8 Development of Radiation Heat Transfer Model:

Developed a model considering radiation heat transfer for pressure tube SCWR extreme accident conditions to more accurately assess thermal-hydraulic responses during accidents.

1.9 Optimization of SCTRAN Calculation Process:

Adopted a modular programming approach to optimize the SCTRAN calculation process, including input/output, basic equation solving, pressure solving, power solving, etc.

1.10 Verification and Testing:

Validated the applicability and accuracy of SCTRAN in supercritical and trans-critical regions by comparing it with internationally renowned programs such as APROS, RELAP5-3D, and CATHENA.

These improvements have significantly enhanced the predictive range, accuracy, and applicability of the SCTRAN program, making it a powerful tool for effectively analysing steady-state and transient conditions, as well as accident analysis and system design in supercritical water reactors. With these enhancements, SCTRAN can better serve the needs of supercritical water reactor conceptual design and safety assessment.

1.11 Application of Supercritical Water Reactor System Analysis Program

1.11.1 CSR1000 Safety Analysis

1) Transient analysis

• Partial loss of main coolant flow

The partial loss of the main coolant flow was caused by the loss of the feedwater pump in the second loop. The main coolant flowrate in this loop was supposed to decrease linearly to zero in 5 s (actually depends on the pump inertia), while the feedwater pump of the other loop maintained the original state. "The low coolant flowrate (90%)" signal triggered the reactor scram signal and RMT actuation at 1 s. After 0.5 s delay, the control rods started to drop and the core power decreased. Figure 1 shows the system parameter variations. The RMT valves were opened after 4.0 s de- lay. The RMT in the second loop quickly drained water into the core by gravity. However, in the first loop, as the main coolant line and the steam line were connected through the RMT and the feedwater pump was still running, part of the feedwater was injected to the steam line, which decrease the coolant flowrate in the first loop. The total coolant flowrate flowing through the core maintained a high level in the first 5 s of the incident and restrained the MCST increase of both passes. The mismatch of core flow and core power increased the MCST of the second pass by 50 ℃. The core pressure kept below the initial values.

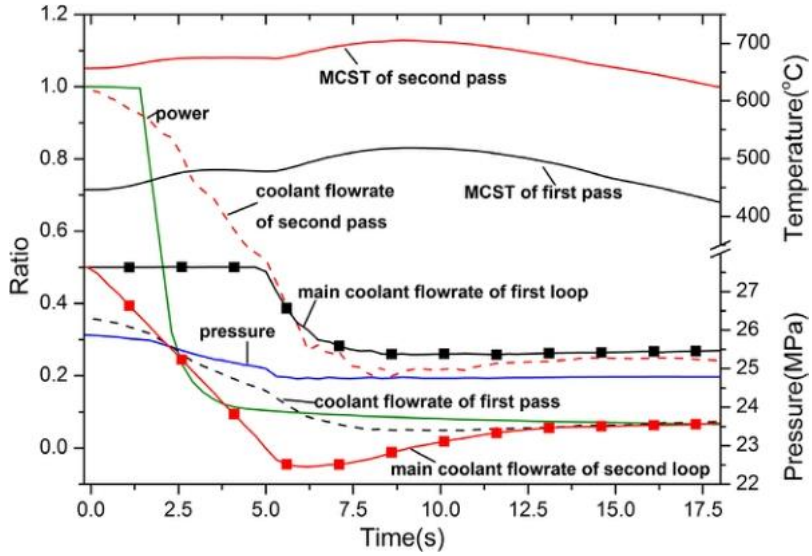

Figure 1. Partial loss of main coolant flow

• Loss of offsite power

In normal conditions of CSR1000, two turbine-driven RCPs were provided to circulate the coolant system. Besides, two motor-driven RCPs were supplied as backups at startup and shut-down conditions. The loss of offsite power did not affect the operation of turbine-driven RCP. In this incident, the ''loss of offsite power'' signal triggered the reactor scram directly. With the supply of steam from moisture separator reheater, the turbine-driven RCPs could keep supplying coolant regardless of the loss of the offsite power. At about 10 s, the steam supplied for the RCPs became less and the RCPs started to run out. Then the ''low coolant flowrate (90%)'' signal triggered the RMT valves to be opened. With the aids of RMT, the main coolant flowrate was maintained to be

about 50% of the original level. During this transient, the MCSTs of both passes stayed below the initial values all the time, as shown in Figure 2.

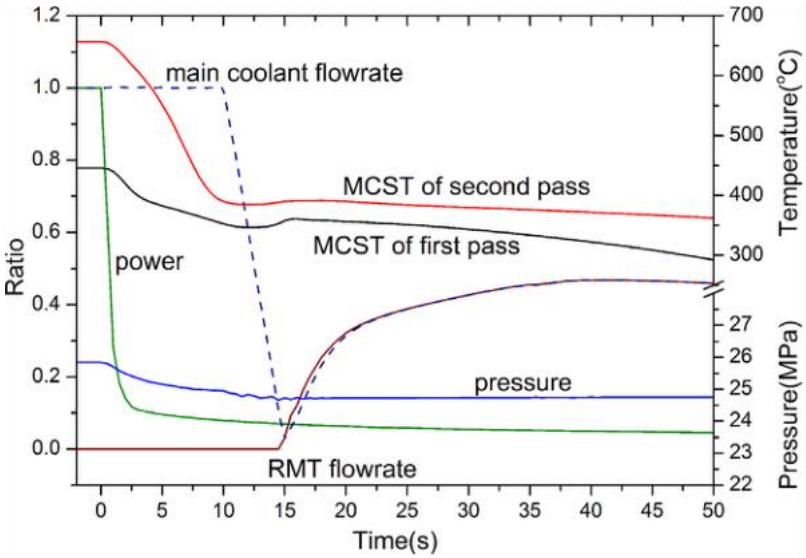

Figure 2. Loss of offsite power

In this transient, the delay time of RCPs trip was decided by the steam supply from the deaerator. The delay time of RCPs trip was an important parameter because it determined when the main coolant flowrate started to decrease. Here a sensitivity analysis of the delay time of RCP trip was performed. Three conditions were simulated, whose delay time were 3, 5 and 10 s separately. The variations of main coolant flowrate and MCST of the second-pass are illustrated in Figure 3. The solid and dotted lines of different colors represent different conditions. From Figure 3 we can see that when- ever the main coolant flowrate started to decrease, the timely intervention of RMT could compensate the coolant inventory in the core. The MCST of second pass stayed below the initial values in all the three conditions due to main coolant flowrate recovery. We can imagine that in the limit case that the delay time equals 0 s, the consequence will be similar to that of "loss of coolant flow- rate accident".

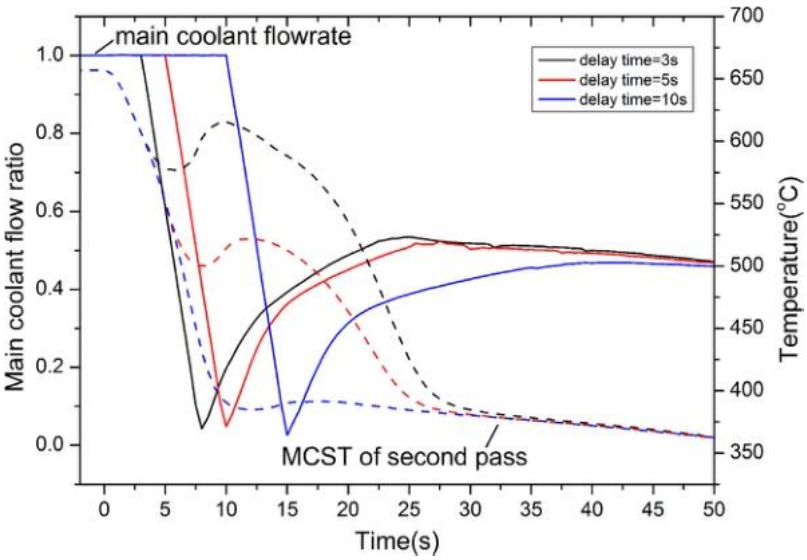

Figure 3. Sensitivity analysis of RCP delay time in loss of offsite power

- **Main coolant control system failure**

This is a typical flowrate increasing incident. The failure of main coolant control system caused the main coolant flowrate increasing to 138% of its original value in 5 s. The simulation re-sult is shown in Figure 4. The increasing coolant flowrate meant that more coolant was injected into the core. The core was better cooled while the cladding temperature and the coolant temperature decreased. Due to the fuel doppler and moderator feedback principle, a positive reactivity feedback was produced. The core power started to increase because of the positive reactivity. It can be observed from the figure that the growth rate of the main coolant flowrate was larger than that of the power. Thus the MCSTs and the coolant temperature decreased, which further in- creased the core power. When the power increased to 120% of its original value, the reactor scram signal was actuated and the power started to decrease after 0.5 s delay. When the reactor coolant pump stopped, the RMTs would be launched and a large amount of cold water was injected to the core, like what happened in the above incidents. The core was effectively cooled and the MCSTs of the both passes stayed below the initial values in the process.

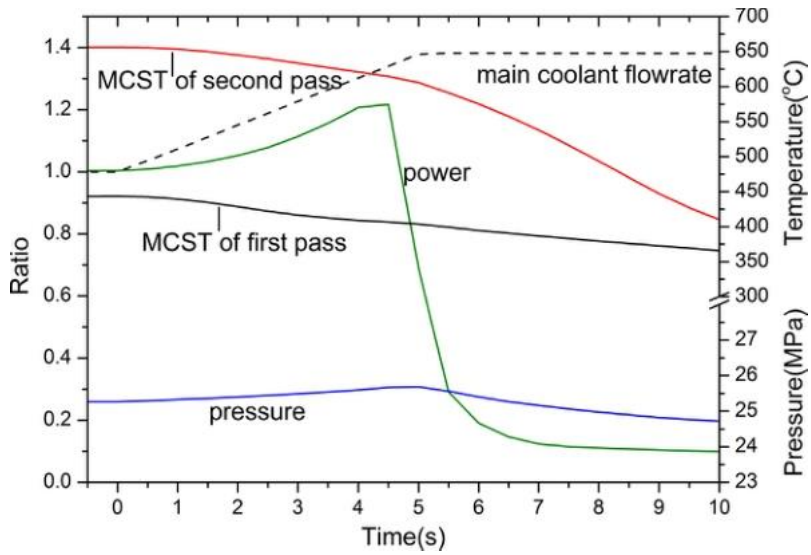

Figure 4. Main coolant control system failure

- **Main steam line valve closure**

In order to observe the safety system response to the abnormal- ities addressing the core pressure, the MSIV closure transient was simulated. The valves of both main steam lines were supposed to be closed in 5 s. The main coolant flowrate was assumed to keep constant in 10 s. The closure of MSIV pressurized the core, which further led to the power scram (high pressure signal). The core pressure reached the threshold value of SRVs and the relief valves were opened to release coolant to avoid overpressure. Thus the core pressure oscillated between 25.02 and 26.72 MPa due to the SRV opening and closing. The flow oscillation amplitude of the second pass was more violent than that of the first pass because of buoyancy effect and drag force in the downward channel. The MCSTs of both passes had a slight increase of 10 ℃, as shown in Figure 5.

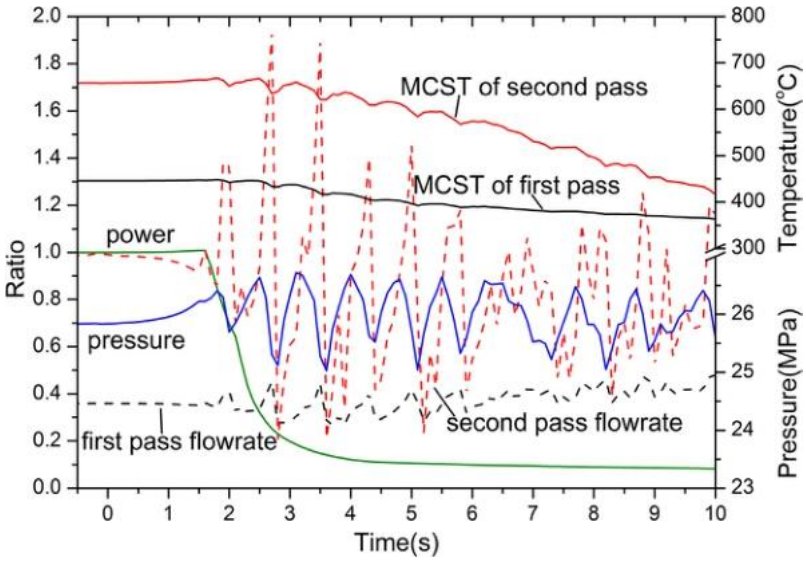

Figure 5. Main steam line valve closure

- **Loss of feedwater heating**

The loss of steam supply to the last high-pressure heater caused the feedwater temperature decreasing from 280 ℃ to 273.6 ℃. The excursion of feedwater temperature was set as 40 ℃ to achieve a conservative result. The result is shown in Figure 6. The temperature decrease of feedwater reduced the coolant temperature and in- creased the coolant density simultaneously. The reactor scram was actuated after the coolant temperature feedback and doppler feedback made the core power rise to 120% of the rated value. The mismatch of the coolant flow and the core power resulted in the cladding temperature increase. The MCST of the second-pass had a peak temperature of 767 ℃.

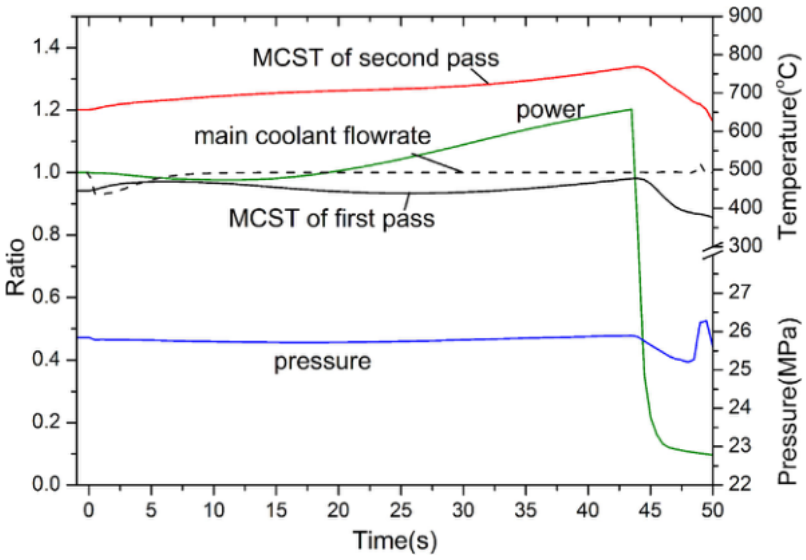

Figure 6. Loss of feedwater heating

- **Uncontrolled CR withdrawal**

The maximum reactivity value of a CR cluster in CSR1000 was not determined yet. The previous literature about the analysis of ‘‘uncontrolled CR withdrawal’ was referred (Ishiwatari et al., 2005a,b). In this simulation, a CR cluster whose reactivity value was 2.0$ was regarded to be drew

out of the core at a uniform speed of 114 cm/min. The core power increased gradually with the CR withdrawal. Thus, the MCST of both passes rose together. When the power reached a certain level, the reactor scram signal was actuated and the power started to decrease after 0.5 s delay. The main coolant flowrate could still maintain for a while and the MCST of both passes started to decrease after reaching a peak value of 750 ℃, as shown in Figure 7. After the coolant pump stopped, the coolant from the RMTs would make up the core flow and cool the core effectively.

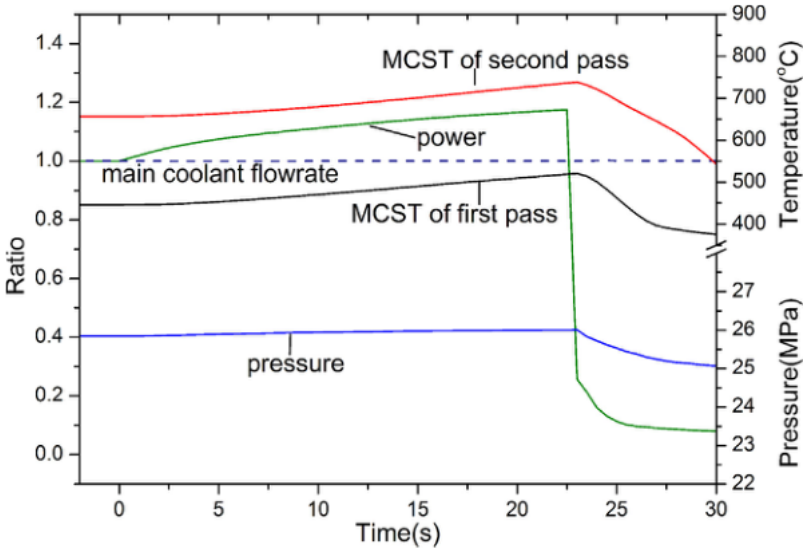

Figure 7. Uncontrolled CR withdrawal

2) Accident *analysis*

• Pump seizure

The consequence of "pump seizure" is shown in Figure 8. In this accident the feedwater pump in the second loop got stuck, which resulted in a sudden loss of the coolant flowrate in 0.1 s. The scram signal was quickly detected because of the "the low feedwater flowrate (90%)". After 4 s delay, the valves of RMT in both loops were opened. Like the process of "partial loss of coolant", the opening of RMT was helpful for the water injection in the second loop while it was disadvantage for the first loop. However, the total coolant was still sufficient to cool down the core after the MCSTs experienced an increase of 100 ℃. This accident was more severe than the "partial loss of coolant flow" because the coolant in one loop lost instantly.

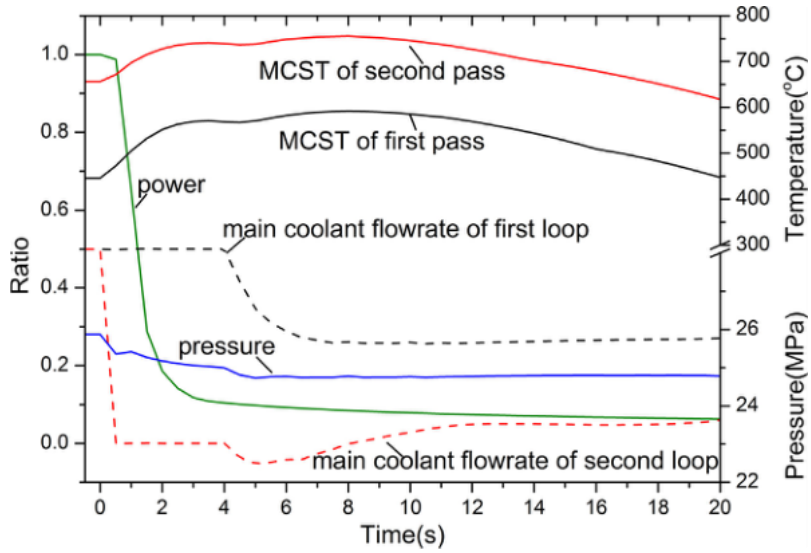

Figure 8. Pump seizure

- **Total loss of coolant flow (LOFA)**

The loss of coolant flow accident (LOFA) was mainly mitigated by the RMT that provided low temperature coolant by gravity in the initial stage and the ICS that cooled the coolant from the core by natural circulation. LOFA was initiated by both RCPs trip. The coolant flowrate was assumed to ramp linearly to zero in 5 s. The "low feedwater flowrate (90%)' signal triggered the scram system and the RMT actuation. The control rods started to insert into the core at 1.0 s and the RMT valve was opened at 5.0 s. From Figure 9 we can see that, in the first 5 s, the mismatch of power and main coolant flow led to the cladding temperature increase. With the injection of cold water from RMT, the coolant flowrate of both passes recovered. The MCSTs of both passes started to decrease after reaching a temperature peak of 815 ℃. The oscillations of system pressure and core flowrate resulted from the open and closure of SRV.

With the draining out of RMT, the ICS valve was opened to provide long-term cooling for LOFA. Figure 10(a) shows clearly that ICS was started at 60 s and the power removed by ICS was larger than the decay heat of the core at about 630 s, which meant that the ICS could provide the long-term decay heat removal. Figure 10(b) shows the coolant flowrate evolutions of both passes with time. When the stable natural circulation was established, the downward flow in the first pass was reversed because of the big flow resistance in the flow channel. The MCST of the first pass had a slight increase in this period. However, it did not change the overall trend of MCST variations. With the startup of the RMT and the ICS in different stages, the MCSTs of both passes decreased and kept being a low level, as shown in Figure 10(c). In the simulation of ICS, the temperature of the ICS pool was set constant.

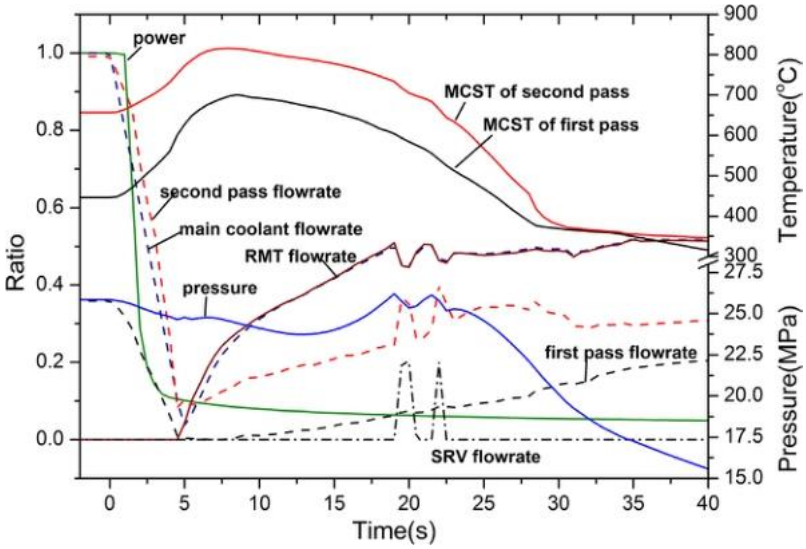

Figure 9. Variations of core parameters in the first 40 s of LOFA

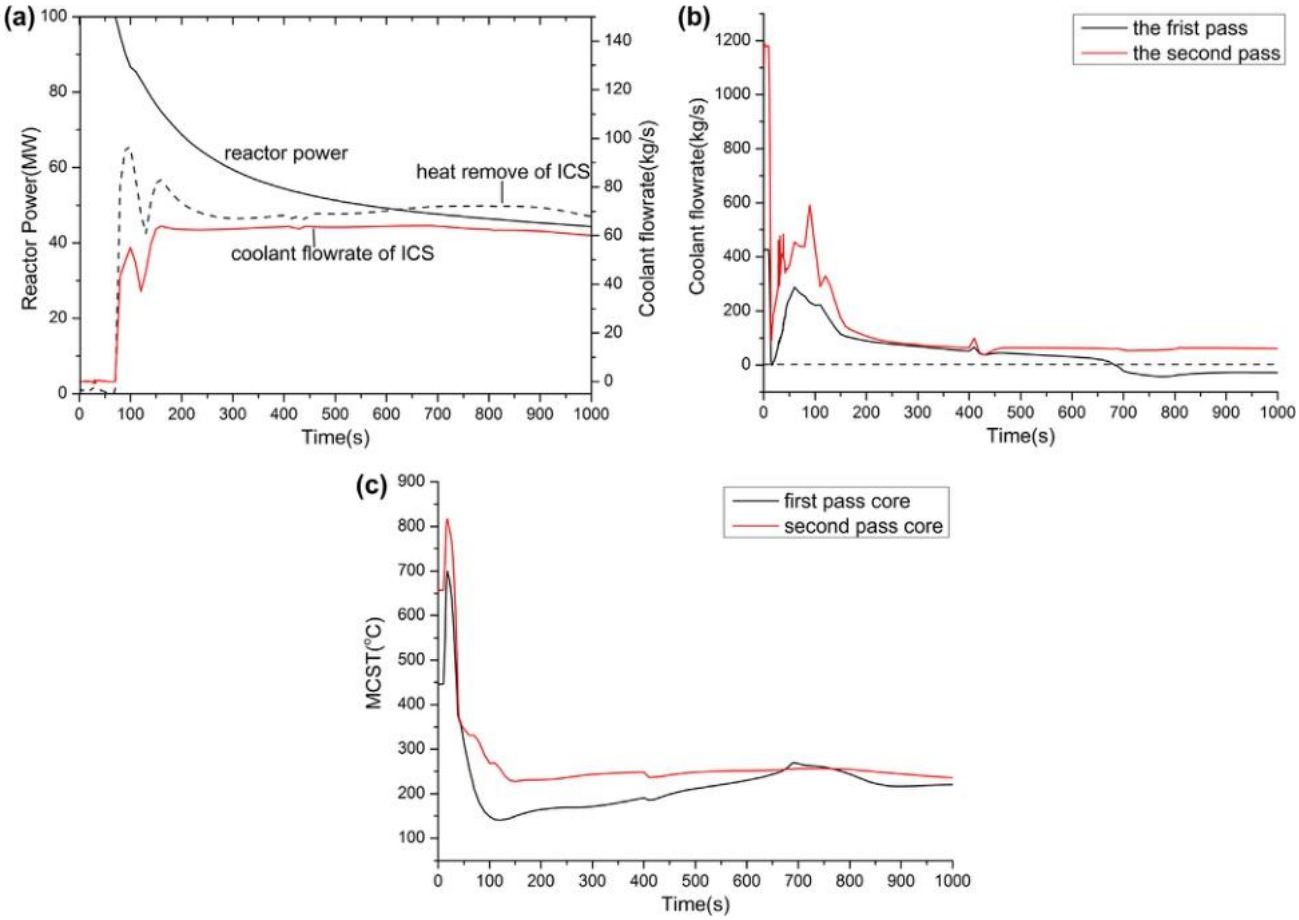

Figure 10. Thermal–hydraulic response in long-term LOFA. (a) The ICS parameters. (b) The core flowrate variations. (c) The MCST evolutions of both passes

From the above analysis, we can realize the importance of RMT in the abnormalities about decreasing in main coolant flow. However, the opening of RMT valve at inappropriate time will make things worse because the feedwater from the main coolant line may flow directly to the main

steam line through the RMT, like the situations of the second-loop in ‘‘partial loss of main coolant flow’’ and ‘‘pump seizure’’. Here a sensitivity analysis about the RMT delay time was conducted for the total loss of flow accident, which was most severe in the abnormalities addressing the main coolant decrease. Four different conditions whose RMT delay times were 0, 2, 4 and 6 s, were simulated. The solid and dotted lines of different colors in Figure 11 represent the variations of the second-pass MCST and the main coolant flowrate in different conditions separately. The main coolant flow decreased most quickly when RMT delay time equaled zero, which resulted in the biggest MCST increase. When delay time equaled 6 s, the core encountered a short period with no coolant injection from RMTs for about 1 s, which was bad for the core cooling. A very good performance was achieved when the delay time equaled 2 s or 4 s. 2 s or 4 s After the reactor scram, the main coolant flowrate dropped to a low level. The water in RMT can flow to the core through the feedwater line by gravity. Therefore, the delay time of RMT should be decided by the main coolant flowrate variation in accidents, which de- pended on the coolant pump inertia. On the premise that the RCP run-down time is 5 s, we regarded 4 s as the best delay time of RMT actuation.

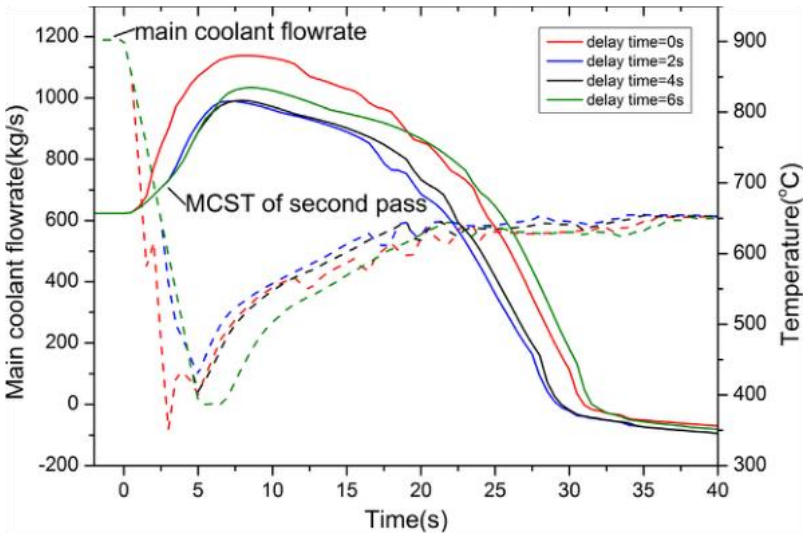

Figure 11. Sensitivity analysis of RMT actuation delay time in LOFA

- **Core depressurization**

This incident was simulated to observe the reactor behavior during the core depressurization. The ADS valves were assumed to be opened at 0 s. The coolant flowed through the ADS valves at a critical velocity. The power scram signal was actuated later because of the low coolant flowrate in the core. The RMT valves were opened at 4 s and the main coolant injection stopped at 5 s because of the pump run-down. At the initial stage of the blow- down phase, coolant in the pressure vessel was led to the steam lines through the two-pass core with the intervention of the ADS. Additionally, the coolant temperature decreased because of the core depressurization (isenthalpic expansion). Thus, the MCSTs decreased quickly. In this period, the coolant from the upper plenum mainly flowed downward through the water rods of the first pass and second-pass other than the first-pass core because there was a big flow resistance in the coolant channel caused by the core heating. That is the reason why the MCST of the first pass started to increase after a slight decrease, as shown in Figure 12(a). In this process, all the coolant gathering in the down plenum had to be directed to the steam line through the second pass core and the MCST of second pass kept decreasing before 30 s. With the blowing out of the coolant, the coolant inventory in the core

became less and the ADS flowrate decreased with the core pressure dropping. The MCSTs of both passes started to increase at about 30 s.

When the pressure dropped to be lower than the containment pressure, which was set 0.2 MPa in this paper, the GDCS pool would take in charge of providing low temperature coolant for the core. In Figure 12(b), the GDCS valves were opened at about 100 s, which means the start of the first reflooding phase. Coolant of low temperature flowed into the DVI lines and cooled the lower plenum. The lower plenum was fully cooled until 230 s. In this period, the MCST of both passes kept rising. After peaking at 850 ℃ and 760 ℃ separately, the MCSTs of both passes started to decrease due to the coolant from GDCS pool entering the core section.

Once the cold coolant entered the fuel channel, it began to cool down the fuel rod and the MCSTs of both passes started to de- crease. Meanwhile, the coolant was heated to steam by the core decay heat, which led to the pressurization of the RPV. The increase of the RPV pressure decreased GDCS flowrate gradually and coolant injection from GDCS was stopped at about 400 s, as shown in Figure 12(b). When the RPV pressure became larger than that of the containment, the coolant in the pressure vessel drained into the containment again through the ADS valves. The flowrate in both passes recovered and the MCSTs kept decreasing. The RPV depressurization started again due to the blowing out of the coolant into the containment. When the RPV pressure was low enough, the coolant injection into the RPV from the GDCS pool (second refilling phase) started. The variations of the MCSTs were similar to those in the first refilling phase. With the decrease of the core power and the starts of the second reflooding phase, the MCSTs of both passes began to decrease after reaching the second peak and finally kept at a low level of around 150 ℃, as shown in Figure 12(c).

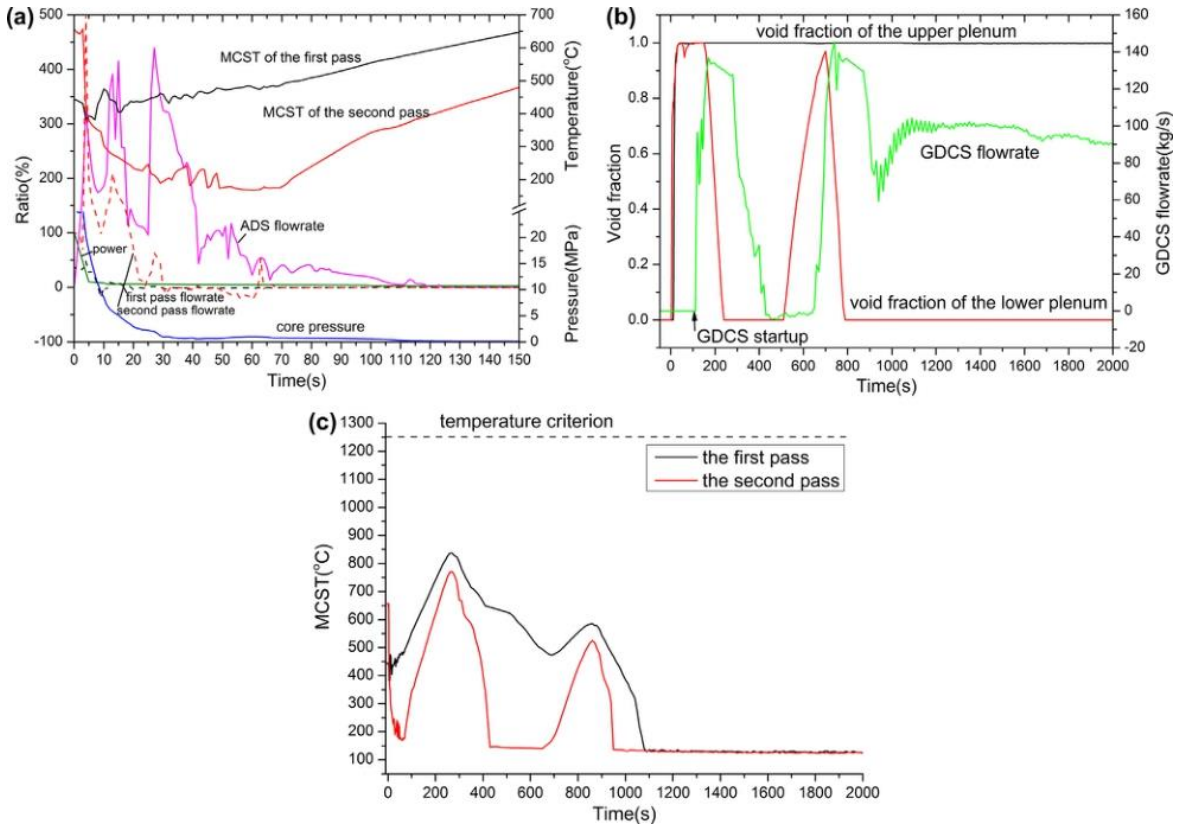

Figure 12. Core depressurization. (a) System parameter variation with time. (b) The void fraction of the lower and upper plenum and the GDCS flowrate. (c) The MCST variation of both passes in 2000 s

1.12 Conclusions

The system analysis program for supercritical water reactors, SCTRAN, utilizes a homogeneous flow model and has been developed based on the power calculation model, heat conduction equations, water state equations, critical heat flux models, heat transfer models, and resistance coefficient models. Written in FORTRAN90, SCTRAN features a modular program structure that facilitates secondary development. It is applicable to both pressure vessel and pressure tube supercritical water reactors and has a broad range of applications, capable of analyzing accidents and transients involving supercritical, transcritical, and subcritical conditions.

A new wide-parameter range wall heat transfer model has been developed to address the numerical discontinuity issues of the original wall heat transfer coefficient during heat transfer mode transitions and the inaccuracy in calculating the heat transfer coefficient above the pseudo-critical point. The new model ensures a smooth transition between heat transfer coefficients, and above the pseudo-critical point, the latest lookup tables are used for calculations, significantly reducing computational errors, especially in the region of post-dried-out film boiling.

The improved system analysis program has been used for safety analysis of the CSR1000, with the computational results meeting the safety limits of reactor design.

2 Customising RELAP5 for SCWR - UNIPI

2.1 Adopted versions of the RELAP5 code

The first part of the work reported in Deliverable D3.3 (Otic et al., 2024) for setting up the nodalisation of the SCW SMR was performed using the NRC version of the RELAP5 Code (SCIENTEC, 1999). As already mentioned in D3.3 and as reported also in Chaaraoui et al. (2024), this version allowed to perform first steady-state analyses of the SCW SMR, but showed serious problems of convergence during depressurizations below the critical pressure.

This represents a classical difficulty encountered by system codes when applied to transcritical conditions, springing from the well-known singularities appearing in fluid thermodynamic properties at the critical point, especially in derivative properties. Several attempts were made to overcome these difficulties by different means, including changing user parameters as time-step and system nodalisation and trying to adopt more refined fluid property tables in the region of the critical point. All these attempts were found useless to obtain the result of a smooth depressurisation from supercritical to subcritical pressures during the postulated long term station blackout (LTSBO) transient, so that a different strategy was conceived.

By the way, as reported in Deliverable 3.2 of ECC-SMART (Zhao et al., 2023), the University of Pisa had promoted an internal benchmark exercise based on the data provided by IPP (Razumovskiy et al., 2008; Razumovskiy et al., 2016) on vertical fuel bundles with 1-rod, 3-rod and 7-rod arrangements and collected by the National Technical University of Ukraine (NTUU). The results obtained by other participants in the ECC-SMART project, i.e., from BME and IPP, making use of their modelling tools, could propose a variety of behaviours obtained with different correlations; on the contrary the University of Pisa, using RELAP5, could test only the correlations already implemented in the code, with little possible choices, leading to somehow predictable results that could not match in any way the observed behaviour of deteriorated heat transfer conditions.

This rather deluding behaviour on both the side of calculation performance at the transition through the critical point and of the little flexibility in the use of correlations led to conceive a different approach, reverting to a version of RELAP5 on which the support of code developers could be obtained.

2.2 Changes made to the RELAP5 code by ISS

As already mentioned in D3.3, a specific cooperation agreement was established with Innovative Systems Software, L.L.C. (ISS) in USA, in order to be allowed to make use of the RELAP/SCDAPSIM code (SCDAP/RELAP5 Development Team, 1998; Allison and Hohorst, 2010), still under maintenance and development, in difference with the frozen NRC version. This allowed to benefit from the cooperation of developers to receive support in solving the numerical problems encountered at the critical point. This decision to revert to RELAP/SCDAPSIM was taken to fulfil the contractual commitment of making use of RELAP5 in the planned analyses, though it was also a good occasion to allow for the improvement of existing modelling tools, to be performed in the frame of the ECC-SMART project and further.

The specific version of the code set up by ISS for this purpose, after some interaction with the University of Pisa, solved the problems encountered during the analysis of the station black-out transient in terms of the impossibility to depressurise the system below the critical pressure. Then,

it was asked to code developers also to provide the user with the possibility to use a generalised heat transfer correlation at supercritical pressure, encompassing the forms of many existing correlations for supercritical fluids, based on the modification of the Dittus-Boelter (1930) relationship by the correction with several property ratios.

The correlation that was asked to ISS to be implemented in the code has the form:

$$Nu = \frac{HTC \times D}{k_b} = [1 + \frac{C}{(x/D_h)^n}] a_1 Re_b^{a_2} Pr_b^{a_3} (\frac{\rho_w}{\rho_b})^{a_4} (\frac{\mu_w}{\mu_b})^{a_5} (\frac{k_w}{k_b})^{a_6} (\frac{C_{p,w}}{C_{p,b}})^{a_7} (\frac{\overline{C_p}}{C_{p,b}})^{a_8} \quad (2\text{-}1)$$

where the coefficients and exponents a_i, C and n can be specified by the user via the input deck for each heating structure.

In this way, the implementation of correlations by Bishop et al. (1965) and Mokry et al. (2011) could be performed in the forms shown hereafter:

- <u>Bishop et al. (1965)</u>

$$Nu = 0.0069 \cdot Re_b^{0.9} \cdot \overline{Pr}_b^{0.66} \cdot \left(\frac{\rho_w}{\rho_b}\right)^{0.43}$$

$$Nu = \frac{HTC \times D}{k_b} = \left[1 + \frac{C}{(x/D_h)^n}\right] a_1 Re_b^{a_2} Pr_b^{a_3} \left(\frac{\rho_w}{\rho_b}\right)^{a_4} \left(\frac{\mu_w}{\mu_b}\right)^{a_5} \left(\frac{k_w}{k_b}\right)^{a_6} \left(\frac{C_{p,w}}{C_{p,b}}\right)^{a_7} \left(\frac{\overline{C_p}}{C_{p,b}}\right)^{a_8}$$

- <u>Mokry et al. (2011)</u>

$$Nu = 0.0061 \cdot Re_b^{0.904} \cdot \overline{Pr}_b^{0.684} \cdot \left(\frac{\rho_w}{\rho_b}\right)^{0.564}$$

$$Nu = \frac{HTC \times D}{k_b} = \left[1 + \frac{C}{(x/D_h)^n}\right] a_1 Re_b^{a_2} Pr_b^{a_3} \left(\frac{\rho_w}{\rho_b}\right)^{a_4} \left(\frac{\mu_w}{\mu_b}\right)^{a_5} \left(\frac{k_w}{k_b}\right)^{a_6} \left(\frac{C_{p,w}}{C_{p,b}}\right)^{a_7} \left(\frac{\overline{C_p}}{C_{p,b}}\right)^{a_8}$$

Concerning the way in which the problems related to the numerical difficulty to perform calculations across the critical pressure were solved, the account received from code developers underlined the fact that the features to operate above critical pressure were already introduced in RELAP5 long ago. The code was in fact mostly prepared for simulating depressurization across the critical point, though it did anyway require some fine-tuning. The actions taken to improve convergence across that sharp discontinuity consisted in introducing fixes in the pre-existing code, without adding any real specific mechanism or technique. Exceptions in evaluating the internal energy of supercritical water, with some specific time-step control options that could lead to unphysical values, and exceptions in the calculation of heat transfer to the gas phase had to be treated in a specific way in the case of supercritical pressures, since a gas phase basically does not exist above the critical point. The event of crossing the supercritical pressure had also to be dealt with better care, to avoid excessive time consumption in the time steps where this event occurred.

While most of the problems involved in the calculation of the LTSBO have been solved, it is foreseeable that the continuing use of the code may give rise to further corrections and fine tuning. The results obtained in the frame of the ECC-SMART project were obtained with a version released to the University of Pisa in July 2023. Examples of the capabilities obtained in the

analyses of the LTSBO have been reported in the mentioned D3.3, together with a first mention to results obtained in a MSc Thesis in Nuclear Engineering (Chaaraoui, 2024) in the comparison with the data by Razumovskiy et al. at NTUU already presented in D3.2 with the use of the NRC version of RELAP5. In the following, an example of its new capabilities is reported in relation to the full data set of the mentioned NTUU experiments, analysed by the Mokry et al. (2011) and Bishop et al. (1965) correlations.

2.3 Reference experimental data from IPP

The following experimental data description is adapted from the one already reported in D3.2. Addressing the interested reader to the document proposed by IPP and to the related literature references by Razumovskiy and collaborators, Figure 13 describes the main geometrical features of the 1-rod, 3-rod and 7-rod configurations adopted in collecting these interesting experimental data. In the test section, the heating tubes (5.2-mm OD and 4.5-mm ID with four helical ribs of 0.6-mm height and 1-mm width) were 485 mm long and were directly heated. The rods in multiple rod bundle configurations are let touching each other. Calibrated 0.1 mm thickness fins were welded to the cylindrical surface of the heaters to provide distancing from a shaped dielectric included in the channel. Water at different supercritical pressures was used in the experiments.

Table 1 summarises the boundary conditions applied in the experiments in terms of working pressure, inlet temperature, mass flux and average heat flux at the heater surface. The values of the overall pressure drops are also reported, though they are not directly addressed in this report.

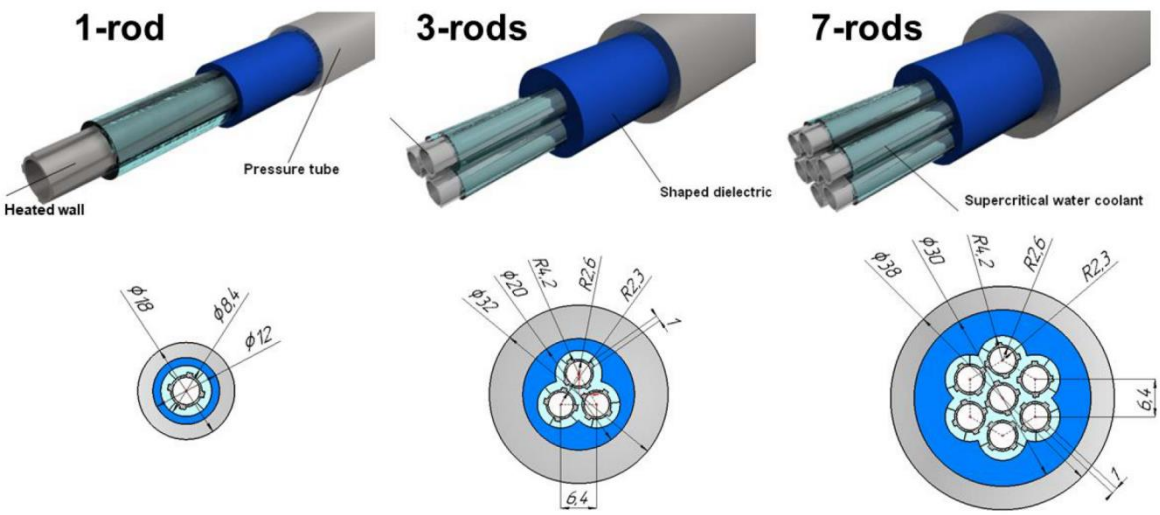

Figure 13. Rod bundle configurations considered in Razumovskiy et al. (2008, 2016)

Table 1. Boundary conditions applied to the bundles during the experiments

Regime No.	Type of bundle	P [MPa]	Tin [ºC]	G [kg/(s*m2)]	qAve, [kW/m2]	ΔP [Pa]
1	#1rod-1	22.6	200	2000	1543	10280
2	#1rod-2	22.6	200	2000	1758	9100
3	#1rod-3	22.6	200	2000	2033	9070
4	#1rod-4	22.6	200	2000	2244	10130
5	#1rod-5	22.6	200	2000	2547	9550
6	#1rod-6	22.6	246	2500	1497	15680
7	#1rod-7	22.6	246	2500	2046	17030
8	#1rod-8	22.6	246	2500	2516	27570
9	#1rod-9	22.6	246	2500	2760	14810
10	#1rod-10	22.6	160	2500	3000	12900
11	#1rod-11	22.6	182	2500	3000	12850
12	#3rod-12	24.5	168	1500	2050	6260
13	#3rod-13	24.5	168	1500	2216	6920
14	#3rod-14	24.5	168	1500	2427	5640
15	#3rod-15	22.6	215	1500	1776	6410
16	#3rod-16	22.6	215	1500	1981	6890
17	#3rod-17	24.5	211	2700	3200	18230
18	#3rod-18	24.5	260	2700	3200	20830
19	#3rod-19	27.5	166	1500	2400	6420
20	#3rod-20	27.5	212	1500	2400	7350

21	#7rod-21	24.5	184	800	719	2800
22	#7rod-22(1)	24.5	184	800	959	3030
23	#7rod-22(2)	24.5	185	800	959	3030
24	#7rod-23c	22.6	178	1000	1288	4295
25	#7rod-23p	22.6	178	1000	1288	4295
26	#7rod-25	24.5	185	800	1067	3190
27	#7rod-27	24.5	246	800	960	3700
28	#7rod-28	22.6	210	800	1180	3440
29	#7rod-29	27.5	210	800	1180	3360

2.4 RELAP5/MOD3.3 nodalisation and calculation procedure

The nodalisation of the system is the one already described in D3.2, whose text is reported here for the sake of convenience for the reader. This nodalisation, used for the NRC version of the RELAP5 code, was not changed in these analyses, only selecting the new correlations by the appropriate input records.

No matter the number of rods included in the test section, the nodalisation adopted for RELAP5 is quite simple, containing the following components:

- an inlet time-dependent volume, adopted for setting the inlet fluid thermodynamic conditions;
- a time-dependent junction, imposing the inlet flow rate while connecting the time-dependent volume and the downstream “pipe” or “annulus” component;
- a vertical pipe or annulus, simulating the heated section and connected to a heating structure; this component has been axially discretised with 97 control volumes having a length of 5 mm each, in order to achieve an axial discretisation accuracy that exceeds by far the one needed or appropriate for discretising such short ducts in production calculations;
- a heating structure, having a cylindrical geometry with inner and outer radiuses corresponding to the nominal inner and outer diameters mentioned in the previous section and wetted on the outer surface; since there is no allowance in the code to consider exactly the geometry of a tube with helicoidal ribs as the ones present on the outer surface of the heaters, the axial length of each one of the 97 heating structures facing the corresponding nodes has been increased proportionally to the ratio of the actual surface area to the theoretical one of the bare heater; the presence of multiple rods in the 3-rod and 7-rod cases has been considered as usual by multiplying the length of each heating structure by 3 or 7

respectively; the heating structures, made by stainless steel, whose properties are available in the code, are radially discretised by 20 nodes;

- a downstream single junction, collecting the flow at the exit of the pipe or annulus component;
- a time-dependent volume, mainly used to specify the outlet pressure, i.e. the gross value of the operating pressure of the system.

After a proper initialization of thermodynamic variables in the system at zero flow rate and power, the flow rate is increased at the time dependent junction in a short duration ramp (from 0 to 10 s), while heating power is also provided to the heater structure by a ramp (from 100 to 200 s). The system is then let to stabilise for additional 100 s, terminating the transient at 300 s from the start, in a sufficiently steady condition. The semi-implicit numerical scheme adopted in the code is used and, owing to the Courant-Friedrichs-Lewy limitation applicable in such case, the timestep is automatically controlled by the code at low values that guarantee numerical stability. The radial heat conduction algorithm is instead fully implicit (possibly, except for the dependence of thermophysical properties of stainless steel by the local value of temperature), so it does not introduce any numerical stability issue.

As for the calculation cases reported in D3.2, since no tool was available to us to represent plots of the RELAP5 computed temperature distributions along the duct axis and along the heated surface, it was necessary to operate copying and pasting the related data from the “major edits” of the code, processing them in a relatively quick way by the aid of an Excel spreadsheet.

With the correlations available at the time of D3.2, the physical options available to the user to be adopted in the calculations, only three choices were tested, corresponding to the use of the hydraulic diameter also for the heat transfer correlations, the use of the heated equivalent diameter in correlations, as allowed by the code. The latter choice was tried because the code allows to use the previous option as a default one, unless the latter equivalent diameter is specifically assigned: so, it was tried to assess which of the two choices could be considered most appropriate for our case. A further option used at the time was related to the use of the heated equivalent diameter plus the option of an “annulus” type of hydrodynamic component in place of the usual “pipe” one. These options, which allowed to discuss the data obtained by the NRC version of the code in front of the user choices allowed at the time, were now superseded by the implementation of the generalised correlation.

2.5 Obtained results

Figure 14 to Figure 16 present the results obtained by the generalised correlation implemented in RELAP5, allowing the user to define the Bishop et al. (1965) and the Mokry et al. (2011) correlations by just changing in the input file the accessible coefficients as shown in previous sections.

As an overall observation on the heat transfer phenomena depicted by the two correlations, it can be noted that also with these two well known correlations, suitable for supercritical pressure conditions, the prediction of deteriorated heat transfer as observed in NTUU data results quite challenging. In particular, no matter the addressed geometry, deteriorated heat transfer is sometimes only mimicked by the correlations, in some cases not exactly with the right boundary conditions. In particular, the Mokry et al. (2011) correlation shows large overestimations of wall temperature with some boundary conditions, with jumps that highlight the existence of multiple

solution branches, as already discussed in D3.3. The older Bishop et al. (1965) correlation shows similar trends, but at much lower extent, this being the reason why it was selected as a more prudent choice for the LTSBO analyses.

It is worth to be clarified that these jumps are not an artifact of the specific implementation in RELAP5, since similar behaviour was found in the results already presented in D3.2, obtained by IPP and BME with their own system codes. On the contrary, this can be shown to be a direct consequence of the form of the two correlations, though it may look quite surprising that the small changes in the exponents of the appearing dimensionless numbers that differentiate the Mokry et al. (2011) correlation from the Bishop et al. (1965) correlation may cause so large discrepancies. Indeed, as already shown in D3.3, a specific implementation of the two correlations in the FORTRAN program adopted for obtaining the results presented in D3.5 (Otic et al., 2024) supports the occurrence of similar results and explains the observed jumps. Actually, it was shown that the presence of multiple solutions in the wall temperature identified by the correlation has the consequence to make any code implementing it to select a possibly stable branch of the available curves, depending on the specific implementation of its thermal-hydraulics and heat conduction algorithms. The great sensitivity to the small changes in the exponents observed in the results may be also a consequence of the operating pressure, in some cases very close to the critical one, giving rise to very sharp changes in fluid properties across the pseudo-critical threshold.

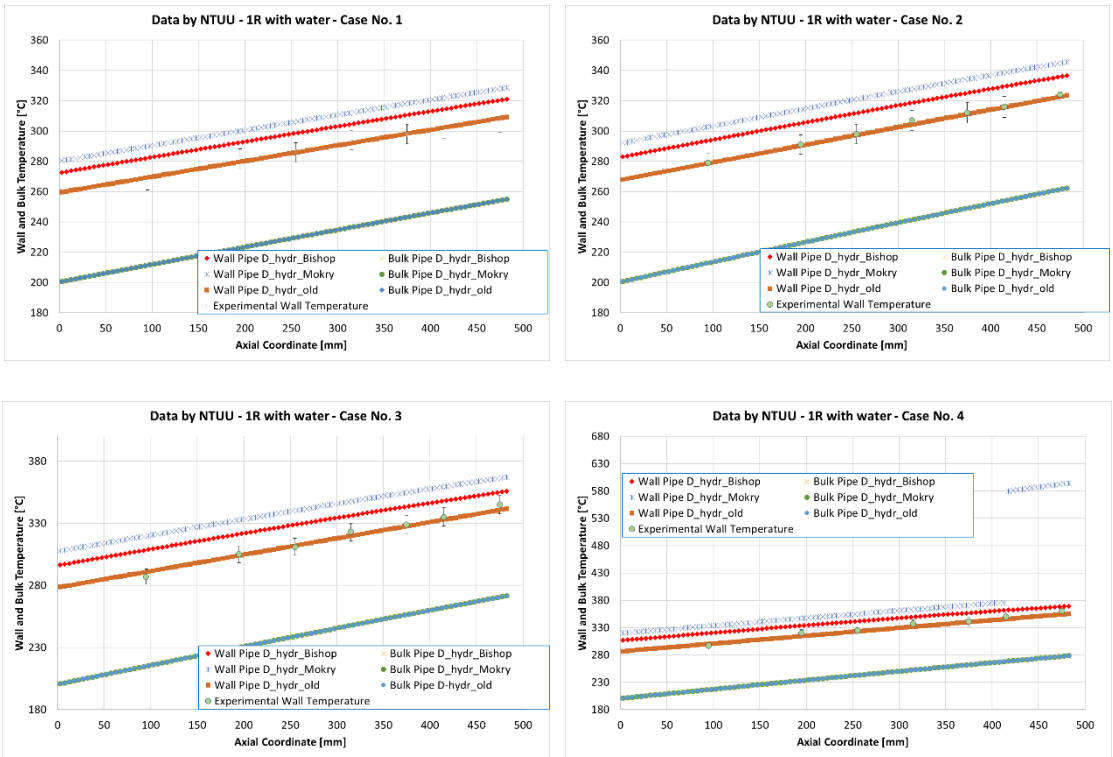

Figure 14. Results obtained with the ISS version of RELAP5 with Mokry and Bishop correlations for 1-rod bundle data from IPP.

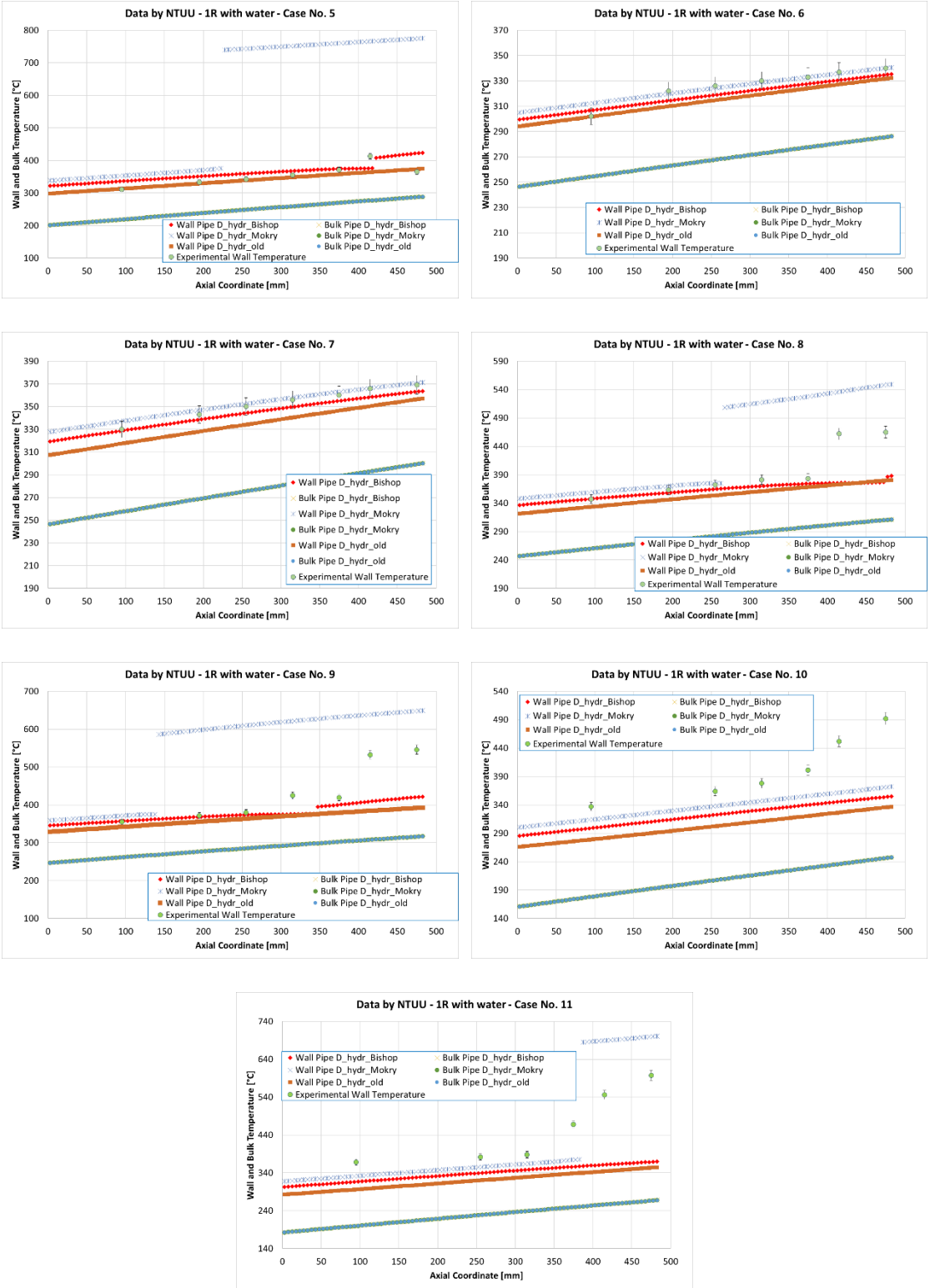

Figure 14. (continued) Results obtained with the ISS version of RELAP5 with Mokry and Bishop correlations for 1-rod bundle data from IPP

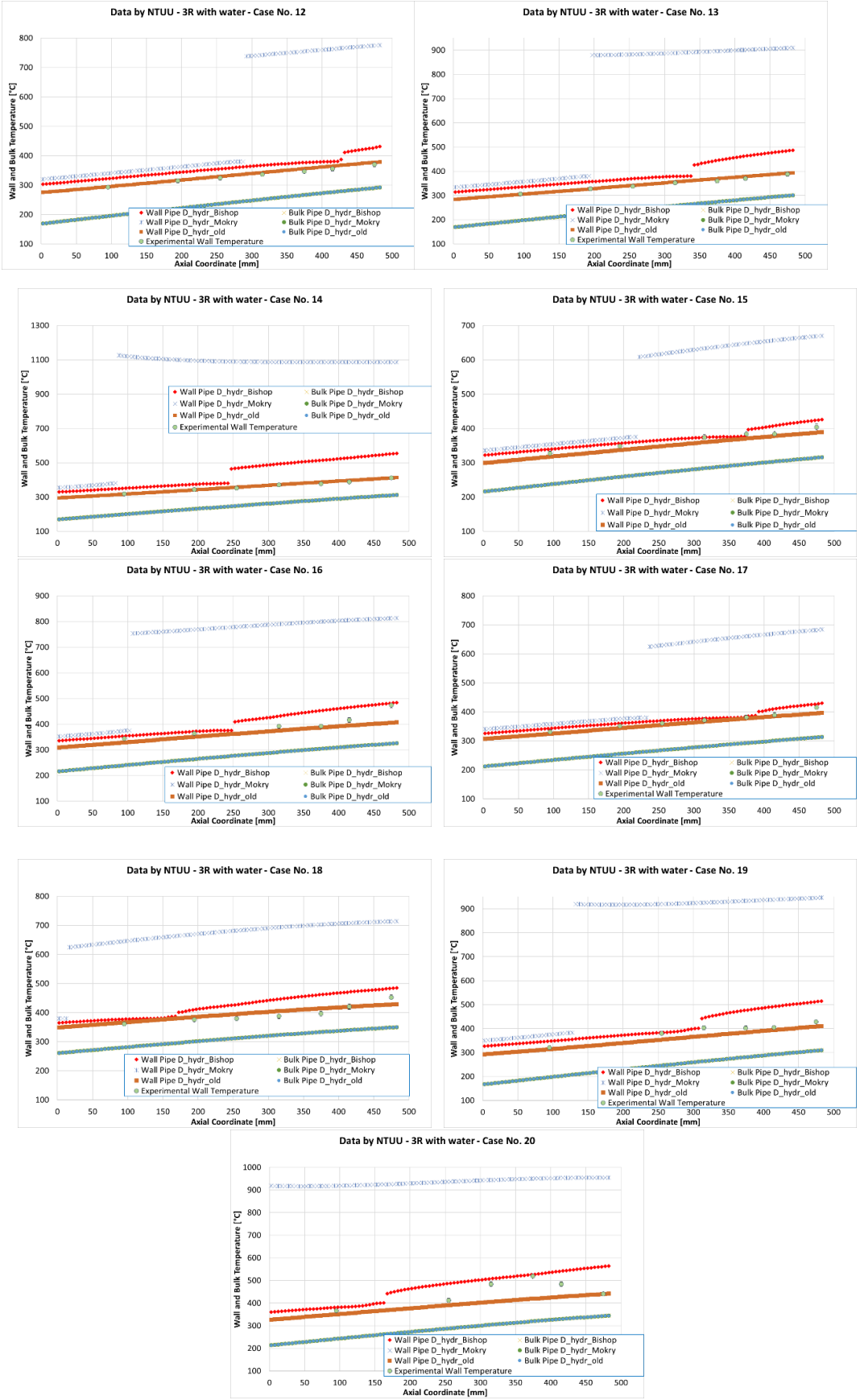

Figure 15. Results obtained with the ISS version of RELAP5 with Mokry and Bishop correlations for 3-rod bundle data from IPP.

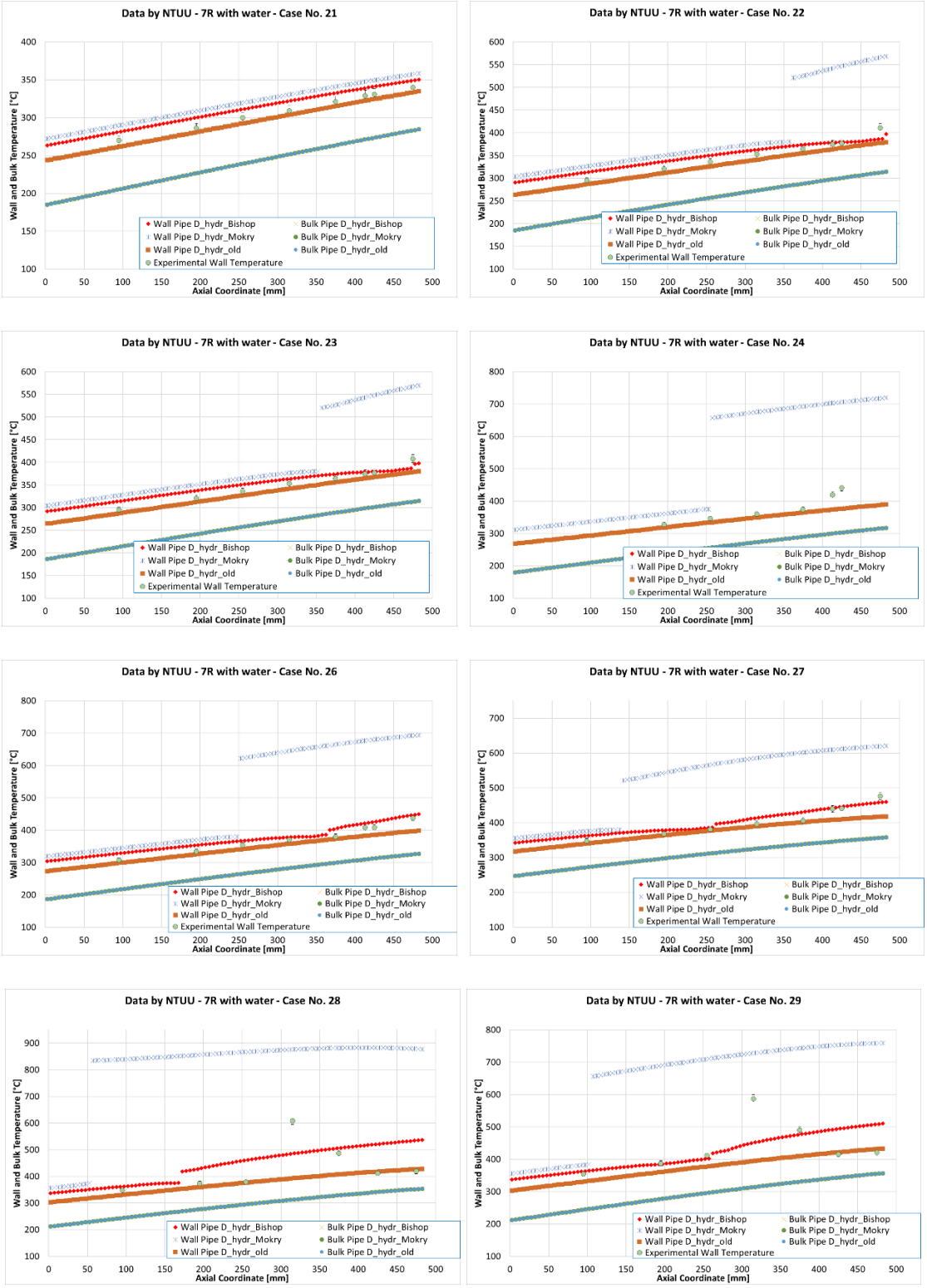

Figure 16. Results obtained with the ISS version of RELAP5 with Mokry and Bishop correlations for 7-rod bundle data from IPP.

2.6 Concluding remarks

The step performed by the University of Pisa in setting up an agreement with ISS for obtaining a developmental version of RELAP5 suitable for performing the targeted LTSBO analysis has provided a new opportunity of applying a well assessed system code to study the characteristics of the design of future SCWRs.

The version presently available to the University of Pisa has been further modified in the frame of analyses performed for assessing stability of heated channels containing supercritical water, to refine the evaluation of fluid properties close to the critical point.

The implementation of a generalised correlation for heat transfer at supercritical pressure opens also to the possibility of sensitivity analyses and to the assessment of new correlations, possibly providing a better accuracy in representing deteriorated heat transfer phenomena that represent a really challenging aspect for the analysis of supercritical water systems.

3 Improvements of the APROS system code for analyses under supercritical pressure conditions - BME

3.1 Modelling supercritical pressure water with APROS

In the frame of the ECC-SMART project, primarily the 6.11.32.02 version of APROS Nuclear system code was used at BME to perform both the benchmark analyses and the simulations related to the proposed SCW-SMR design.

APROS has been able to work with supercritical (SC) pressure water for more than 15 years, and has been used many times for modelling of SC systems (Kurki, 2008; Hänninen et al., 2009; Li et al., 2014; Yan et al., 2014, etc.), and in particular for the analyses of the HPLWR concept (Kurki and Seppälä, 2009; Schlagenhaufer et. al, 2010; Andreani et. al, 2012). The thermal hydraulic solution for SC conditions is based on the standard two-phase models, but includes various modifications. Some parameters had to be redefined because of their different physical significance at the subcritical pressures, the steam tables had to be improved and extended, while a pseudo-phase-transition had to be introduced at supercritical pressures. Now, APROS uses an approximate implementation of the IAPWS-IF97 formulation for the calculation of the thermo-physical properties. Additional heat transfer and friction correlations were also required for the new regions (Kurki, 2008; Hänninen et al., 2009).

Several thermal hydraulic models are available in APROS for two-phase calculations, two of which are most commonly used: the homogeneous (3-equation) and the two-fluid (6-equation) model. The first assumes that the phases share a common temperature and velocity, while the second treats the phases as separate fluids. The homogeneous model might seem to be ideal for SC conditions as the fluid stays in one phase. However, it would give unacceptable results during transients, if the pressure drops suddenly to subcritical conditions. Consequently, the 6-equation model is generally preferred for the supercritical conditions.

Constitutive equations are also needed to solve the above governing equations. The skin friction factor correlation of Kirillov (Pioro et al., 2004) was chosen and implemented in APROS for the supercritical pressure region. Numerous heat transfer correlations for the supercritical pressure conditions are available in the literature. Five of these were found to be the most suitable for the simulation and thus implemented for the 6-equation model by the APROS developers. These are the following: Bishop et al., 1965; Jackson et al., 1979; Dittus et al., 1930; Mokry et al., 2010; Watts et al., 1982.

In case of the homogeneous model, a specific heat transfer correlation for the supercritical region cannot be selected. However, the user has the possibility to implement and use an own defined heat transfer correlation. To be able to compare the behaviour of the homogeneous and the 6-equation models, the above given five and the (Dyadyakin and Popov, 1977) heat transfer correlations have been implemented in APROS by BME. The Bishop and the Jackson and Hall correlations have an alternative form, which includes an additional “entrance term”. The implementation made it possible to use them with or without this additional term. Some of the heat transfer correlations require the coolant properties also at the wall temperature (e.g. ρw), which is not directly extractable from APROS’s steam table. To be able to define such correlations, an own steam table function (based on the IAPWS-IF97 formulation) had to be implemented by BME, with which the required properties can be calculated in runtime.

To solve the above presented system of partial differential equation, they need to be discretized with respect to space and time, and the nonlinear terms need to be linearized. In the space discretization, the staggered discretization scheme and finite difference method is applied. This discretization then leads to an algebraic equation system, which is solved using an iterative pressure-correction algorithm.

3.2 Improvement of the APROS code based on the benchmarking

A summary of the benchmark analyses performed by BME with APROS in the frame of the ECC-SMART project is presented in Deliverable D3.2 and in a journal paper (Varju et al., 2024). This benchmarking activity covered the whole set of the NTUU rod bundle data, most of the NTUU bare tube data, as well as Yamagata's and Bazargan's bare tube data, provided by IPP. With the finalised models, described in D3.2, a series of steady-state calculations have been performed using the boundary conditions of the experimental regimes. These calculations have been performed both with the homogeneous and the 6-equation model, and with all of the built-in and self-implemented heat transfer correlations.

As described previously, the 6-equation model uses the built-in correlations and steamtable, while the 3equation model uses the user defined versions of these. After the simulation of the first few NTUU test cases, the obtained results were compared, and a significant difference was found between the 3-equation and 6-equation model results in regimes with high wall – bulk temperature difference. BME contacted the APROS developers with this observation and it turned out to be a result of a fixed limitation of the built-in correlations, which was not assumed in the user defined versions. The (ρw/ρb) density ratio had a minimum value of 0.2 that roughly corresponds to a maximum of 50 °C temperature difference (near critical point and 400 °C temperature). In the NTUU experiment, the wall - bulk temperature difference exceeded this limit significantly, and thus the built-in correlations suffered from the limitation.

As a result of the discussions with the developers, BME received a modified Beta version of the related DLL for APROS version 6.11.32.02, in which the minimum value of the density ratio has been decreased to 0.08. From APROS version 6.12 onwards, the new limit value is used by default.

Finally, all of the considered benchmark cases was analysed with the new, improved code version, the results of which are presented in D3.2 and in (Varju et al., 2024). However, a few examples are given in Figure 17 and Figure 18 to show the difference caused by the original limitation.

The most significant effect is seen in case of the Bishop correlation, while the Dittus-Boelter did not change at all, because it does not have a (ρw/ρb) ratio term. With the new DLL, the simulation results got much closer to the measurements and the significant difference, experienced earlier between the 3-equation and 6-equation models, has disappeared. It confirms two important findings:

- The reason for the discrepancy was successfully found and the code needed to be corrected to be used for supercritical calculations with high wall - bulk temperature difference.
- The heat transfer correlations and steam-table implementation of BME is correct and can be used in later applications.

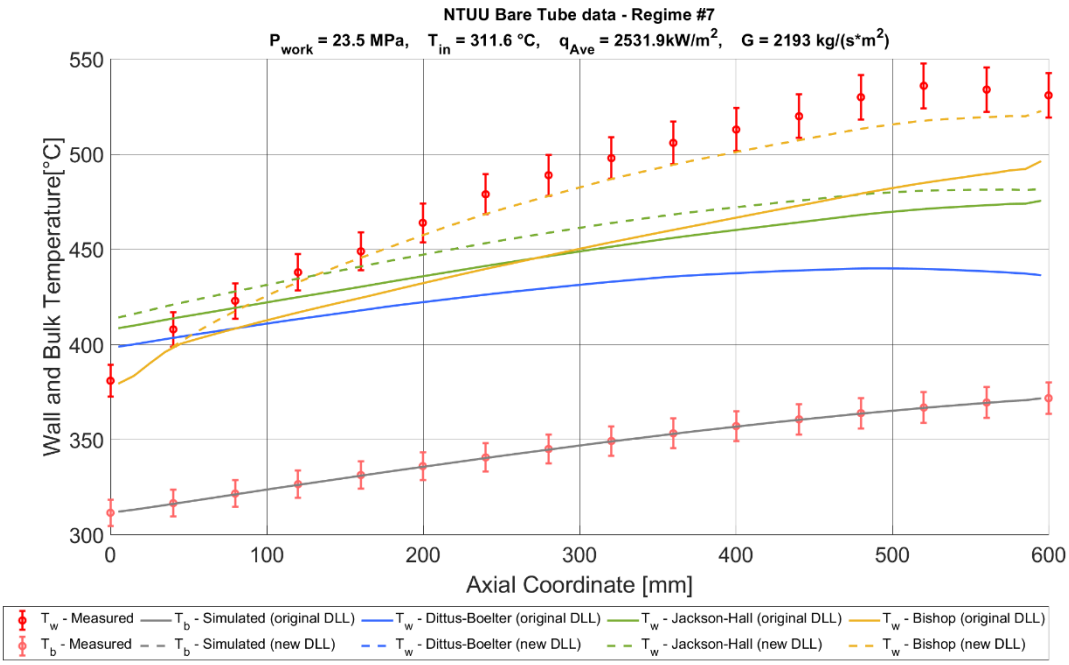

Figure *17* Wall and Bulk temperature results of a bare tube case with the original and the new DLL

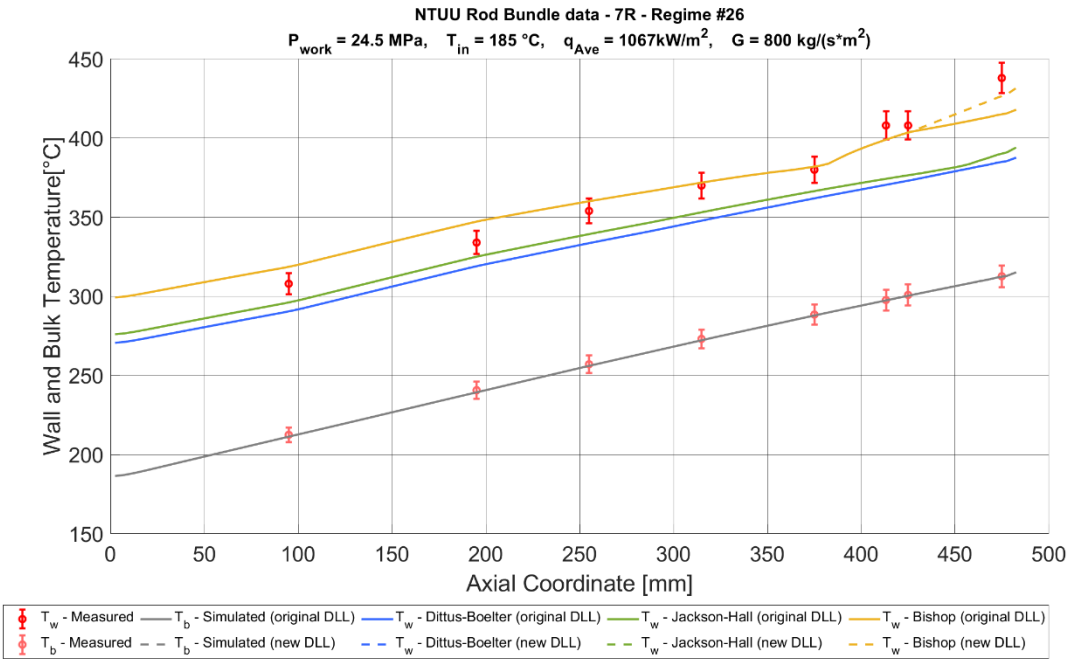

Figure *18* Wall and Bulk temperature results of a rod bundle case with the original and the new DLL

In addition to the code improvement described above, BME also asked the APROS developers to provide users with the ability to implement their own supercritical heat transfer correlations also for the 6-equation model in the future, if possible. The developers accepted this request, and efforts will be made to provide this possibility in the future.

3.3 Concluding remarks

During the benchmark analyses carried out at the BME, an inappropriate limitation in the built-in heat transfer correlations of APROS was discovered, which resulted in unrealistically high heat transfer coefficients and thus too low cladding temperatures in regimes with high wall – bulk temperature difference. With the help of the code developers, the value of this limitation was significantly reduced, and the results of the improved code are now correct.

During further benchmarking activities and various stand-alone and coupled steady-state and transient analyses performed with APROS on the proposed SCW-SMR concept (see Deliverable D3.3), the code and the developed models worked properly, and no unexpected or unexplained issues were encountered. The various APROS results were consistent with each other and with those of the RELAP models developed by UNIPI. During transient analyses with a significant drop of the system pressure (e.g. SBO), when the supercritical - subcritical pressure wave propagates through the entire model, the calculation slows down considerably, but remains stable in all cases studied and no convergence issues were encountered. Based on the above, APROS proved to be quite stable under the specific conditions investigated, no further problems were discovered, and therefore no further corrections or improvements were required.

4 Adaptation and improvement of Transfer Matrix Method for analyses the flows with SCP - IPP

4.1 Introductory remarks

The one-dimensional flow system of a non-isothermal medium, with consideration of phase transitions, is the basis of many system codes for improved thermal hydraulic estimation (RELAP, TRACE, ATHLET, APROS, KORSAR etc.), which are now being adapted for the calculations of flows under super critical parameters (Zhang et al., 2020; Zhou et al., 2012; Jäger et al., 2011).

In many cases, when an elementary channel is considered, the problem is reduced to transcendental balance equations, which are obtained by neglecting local effects and insertion of mass average values. The extremely nonlinear behavior of thermophysical properties at the SCP near the point of pseudo-phase transition is one of the reasons for the thermal acceleration occurrence, which cannot be neglected. In addition, there is still a problem of the modern implicit correlations robustness (IAEA-TECDOC-1746), which give excellent agreement with experiment during a priori evaluation, but do not converge at all in many cases (Varju et al., 2024) when they applied implicitly (determining values - the bulk and wall temperatures). And even if the results are convergent, they cannot always be interpreted correctly. Obtained results may indicate the presence of a heat transfer deterioration, which may be correct. At the same time, an “inlet” peak may appear on the axial profile of the wall temperature, which is a consequence of the solution discontinuity (if the method allows), but is not a physical reproduction of the velocity profile restructuring. This issue of the applicability of existing correlations was considered in more detail by the project participants - UNIPI, BME and IPP in the framework of joint work (Varju et al., 2024). Also, problems with convergence often arise when applying system codes to modeling the depressurization and overcoming the point of pseudophase transition.

Therefore, in order to solve the listed problems, IPP concentrated their efforts on the following:

- At first stages IPP performed the adaptation of transfer matrix method for the analysis of non-linear thermal hydraulic processes (Filonov et al., 2022) using successful experience of beam approximation approach (briefly described in section 4.2).
- In order to generalize the understanding of the HTC correlations applicability, the entire set of 59 available correlations formed by UNIPI (Kassem et al., 2022) was implemented by IPP in TMM. Due to the efficiency and calculation speed of the adapted method, it was possible to test the applicability of these correlations on the entire available data set collected by IPP in the ECC-SMART database (described in deliverable D.3.1 and deliverable D.3.2). This work included testing each correlation on experimental data for supercritical water flow in vertical/horizontal bare tubes, and on regimes with vertical flow in rod bundles. In result of this work, the HTC correlations "robustness maps" were prepared. Their brief description and application results are provided in section 4.3.
- Next, IPP proposed and developed a non-linear differential method for predicting the intensity of heat transfer and energy dissipation at supercritical parameters of the coolant, which is based on the "narrow channel" model (see description in section 4.3). In essence, the developed method can serve as a replacement for HTC and PLF correlations. According to the obtained

results, in combination with the TMM method, it significantly improves the possibilities of predicting regimes with HTD phenomenon.

4.2 Adaptation of TMM for analyses heat transfer regimes with extremely nonlinear behavior of thermophysical properties

At first stage the work of IPP was aimed at generalizing the successful experience of Transfer Matrix Method application previously used for beam approximation and adopt it for continuous supercritical medium flow problems in the one-dimensional approximation. This section describes the main features of the transfer matrix method (TMM) adaptation for a non-isothermal supercritical flow with extremely non-linear thermophysical properties.

To linearize the original system of equations, the concept of transitional ("basic") and "correction" solution is proposed (Filonov et al., 2022). The equations for the "correction" values, which actually characterize the residual with the "basic" parameters for the elementary section, are solved exactly. Application of this method allows to build an unambiguous connection between the «inlet» and «outlet» boundaries of the pipeline for the "correction" value. Also this method allows to remove restrictions on the type of empirical correlations of the pressure loss and heat transfer coefficients, which is quite important in the case of generalizations for the supercritical medium.

Verification of the method is described in (Filonov et al., 2022). The proposed method stability and validation are described in short in section 7.2.2. For this the NTUU data from experimental database (see description in deliverables D3.1 and D3.2) was used. The method application was tested using several implicit empirical correlations, for which it is difficult to obtain a convergent solution for some regimes using classical approaches.

4.2.1 General description of the accepted formalism and the concept of adaptation

Transient processes of a single-phase medium transfer in the one-dimensional approximation can be represented as a nonlinear equations system (4-1). A feature of the system (4-1) is that n-k equations are differential, and the rest k are algebraic (generally transcendental). Usually differential equations describe conservation laws, and algebraic/transcendental - equations of state. Therefore, the vector of unknowns $\vec{\Pi} = \vec{\Pi}^d \bigcup \vec{\Pi}^a$ has coordinates in the form of variables, each of which belongs to the equation of system (4-1) that characterize it.

$$\begin{cases} \dfrac{\partial(\rho f)}{\partial t} + \dfrac{\partial}{\partial x}(\rho w f) = \Gamma_G \\ \dfrac{\partial(\rho w f)}{\partial t} + \dfrac{\partial}{\partial x}\left(\rho w^2 f\right) = -f\dfrac{\partial p}{\partial x} - \rho g f \cdot \cos(\theta) - \xi \rho w |w| P_h - \Gamma_p \\ \dfrac{\partial}{\partial t}\left[\rho\left(\varepsilon + \dfrac{w}{2}\right) f\right] + \dfrac{\partial}{\partial x}\left[\rho w\left(\varepsilon + \dfrac{w^2}{2}\right) f\right] = -\dfrac{\partial}{\partial x}(p w f) - \rho g f w \cdot \cos(\theta) + \dfrac{\partial}{\partial x}\left(\lambda \dfrac{\partial T}{\partial x} f\right) - \phi(T, T_{wall}) + \xi \rho w^2 |w| P_h - \Gamma_T \\ \phi(T, T_{wall}) = P_t \cdot HTC \cdot (T_{wall} - T) = P_t \cdot q \\ \rho = \rho(p, T) \\ \varepsilon = \varepsilon(p, T) \end{cases} \quad (4\text{-}1)$$

where, p – absolute pressure, w – longitudinal velocity, T – the temperature of the supercritical medium, P_h and P_t – hydraulic and heat perimeters, ρ – density, ε - internal flow energy, $\Gamma_G, \Gamma_p, \Gamma_T$ - functions of interchannel exchange of mass, momentum and energy, f – cross-sectional area of

the channel, Φ – function of external heat exchange, T_{wall} – wall temperature, cos (Θ) – specifies the orientation in space.

Since the original system is nonlinear, it is important to describe the approach by which the solution was constructed. To simplify the demonstration of the method application, we consider the channel approximation in a steady-state formulation (simple pipe), in which there is no transverse exchange, i.e. $\Gamma_G, \Gamma_p, \Gamma_T$ are equal to zero. Generalization to the transient case practically does not change the essence of the approach.

For ease of description, we present the original system (4-1) in a generalized form as follows:

$$\begin{cases} A_i^j\left(\vec{\Pi}\right)\cdot L_t\left(\Pi_i\right)+B_i^j\left(\vec{\Pi}\right)\cdot L_x\left(\Pi_i\right)+C_i^j\left(\vec{\Pi}\right)\cdot L_{xx}\left(\Pi_i\right)=F_j\left(\vec{\Pi}\right) \\ \left\{L_t;L_x;L_{xx}\right\}=\left\{\dfrac{\partial}{\partial\tau};\dfrac{\partial}{\partial x};\dfrac{\partial^2}{\partial x^2}\right\} \\ i,j=1..n \end{cases} \tag{4-2}$$

The vector $\vec{\Pi}^d$ contain the coordinates of only those variables that are characterized by differential equations (for example – velocity, pressure, temperature), and the vector $\vec{\Pi}^a$ - by the rest (internal energy, density and external heat transfer function). In most practical problems related to non-isothermal flow, the $\vec{\Pi}^a$ vector of variables can be represented as $\Pi_i^a=\Psi_i\left(\vec{\Pi}^d\right), i=1..k$ (e.g. density expressed as a function of pressure and temperature). For convenience, the $\vec{\Pi}^d$ vector of variables is called “basic”, and $\vec{\Pi}^a$ - "auxiliary".

The solution for n-k "basic" variables is represented in the series form (4-3), where $\Pi_{i,0}^{base}$ - assumed solution (initial approximation), Π_j^{cor} - adaptive “correction” value.

$$\Pi_i^d=\Pi_{i,0}^{base}+\sum_{j=1}^{m}k_j^{dyn}\cdot\Pi_j^{cor} \tag{4-3}$$

To determine Π_j^{cor}, the system (4-2) is linearized with respect to the variables of the $\vec{\Pi}^d$ vector. Each of the coordinates is represented as a sum of the "basic" and "correction" values: $\Pi_i^d=\Pi_i^{base}+\Pi_i^{cor}\Leftrightarrow\partial\Pi_i^d=\partial\Pi_i^{base}+\partial\Pi_i^{cor}, i=1..n-k$. The main rules of such linearization described in more details in (Filonov et al., 2022).

After linearization process, the system (4-2) can be reduced to a system of linear inhomogeneous differential equations with variable coefficients:

$$\begin{cases} \tilde{A}_i^j\left(x\right)\Big|_{base}\cdot L_x\left(\Pi_i^{cor}\right)+\tilde{B}_i^j\left(x\right)\Big|_{base}\cdot L_{xx}\left(\Pi_i^{cor}\right)+\tilde{C}_i^j\left(x\right)\Big|_{base}\cdot\Pi_i^{cor}=R_j\left(x\right)\Big|_{base} \\ i,j=1..n-k \end{cases} \tag{4-4}$$

Where, the function $R_j\left(x\right)\Big|_{base}$ - looks exactly like the n-k differential equations of the system (4-2). In fact, the right part of (4-4) can be interpreted as an imbalance of the system (4-2) presented in terms of "basic" and "correction" values. System (4-4) can be solved in various ways, for

example, by minimizing the absolute value of the right side of (4-4), which in the limiting case will ensure the fulfillment of (4-2). This is partly similar to FEM.

To solve (4-4) with respect to the "correction" values, the elementary geometric section [x_k; x_{k+1}] with a length δx_i is considered (see Figure 19). Within this elementary section the coefficients for the "corrective" values are assumed to be constant. Then, the system of equations (4-4) can be solved by analytical or hybrid methods (analytics + finite differences) on each elementary section and connections between the inlet and outlet boundaries of elementary section can be represented in matrix form:

$$\vec{\Pi}^{cor}\left(x_{k+1}\right)=\left[A_{local}^{solve}\left(\delta x_k\right)\right]_{base}\vec{\Pi}^{cor}\left(x_k\right)+\left[B_{local}^{solve}\left(\delta x_k\right)\right]_{base} \tag{4-5}$$

This is one more similarity with FEM, except that the shape function on an elementary section for the "correction" value is "exact" in the proposed approach.

Figure 19 shows the schematic illustration of the "basic" and "correction" values determination for the elementary section.

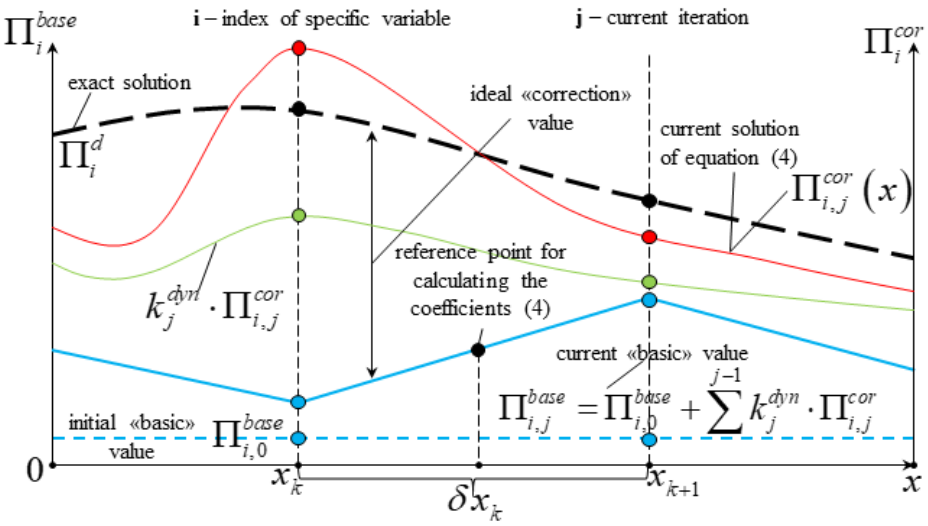

Figure 19. Illustration of the "basic" and "correction" values on the elementary section for the current iteration

4.2.2 Demonstration of stability of the proposed method

As an example of the TMM application, two steady state regimes of heat transfer with supercritical coolant parameters (extremely non-linear thermal properties) in a bare tube are considered. To calculate the intensity of heat transfer, the correlations of Chen&Fang (4-6), and Razumovskiy (4-7) are applied. The friction resistance coefficient is calculated according to the equation (4-8).

$$HTC_{C\&F} = \frac{k_b}{d} \cdot 0.46\,\mathrm{Re}_b^{0.16} \left(\frac{\mathrm{Pr}_w}{\mathrm{Pr}_b}\right)^{0.1} \left(\frac{\nu_w}{\nu_b}\right)^{-0.55} \left[\frac{h_w - h_b}{(T_w - T_b)\cdot c_{pb}}\right]^{0.88} \left[\frac{\beta_b \rho_b d \cdot q}{(\rho_b - \rho_w)\cdot k_b}\right]^{0.81} \tag{4-6}$$

$$HTC_R = \frac{k_b}{d} \cdot \frac{0.81 \cdot \left(\xi_{fr}/8\right) \mathrm{Re}_b\,\mathrm{Pr}_b}{1.07 + 12.7\sqrt{\xi_{fr}/8}\left(\mathrm{Pr}_b^{2/3} - 1\right)} \left[\frac{h_w - h_b}{(T_w - T_b)\cdot c_{pb}}\right]^{0.63} \tag{4-7}$$

$$\xi_{fr} = \left(1.82 \cdot \log_{10}\left[\frac{\mathrm{Re}_b}{8}\right]\right)^{-2} \left(\frac{\mu_w}{\mu_b}\right)^{0.15} \left(\frac{\rho_w}{\rho_b}\right)^{0.1} \tag{4-8}$$

Application of the Chen&Fang correlation allows to demonstrate the problem, since in the a priori estimate it gives excellent agreement with the experimental HTC, and when it is used implicitly, difficulties with convergence often arise (Varju et al., 2024). Even in case of obtaining the solution, the temperature profile differs significantly from the experimental one and can be misinterpreted in the safety analysis. Usually this is due to the fact that the correlation is ambiguous. If we consider the curve of intersection the $q = const$ and $HTC \cdot (T_w - T_f) - q = 0$ surfaces in $(T_b; T_w; q)$ coordinate system, then it must be a single-valued function (Figure 20).

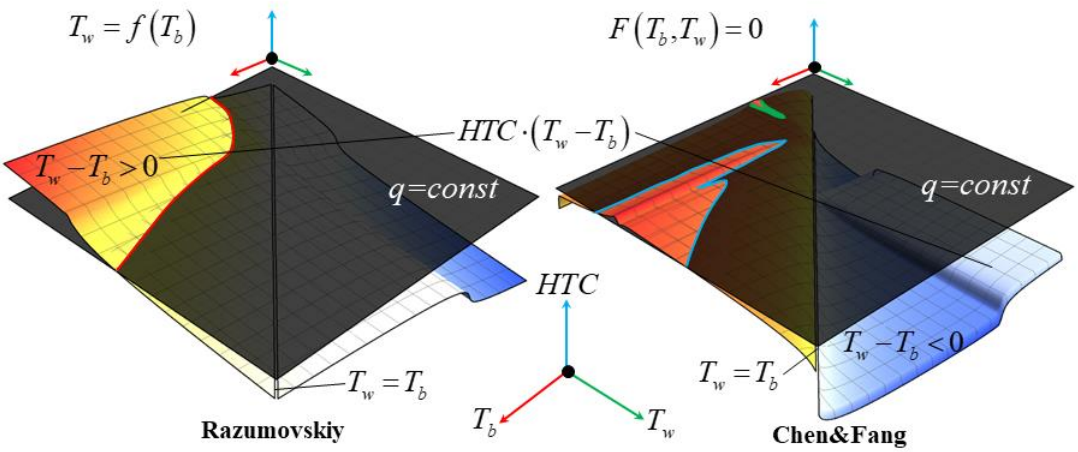

Figure 20. The problem of implicit correlations unambiguousness

As considered experimental cases two regimes from NTUU data with upward flow direction of supercritical fluid through a pipe of 4 m high with an outer diameter of 0.01 m are analysed.

For both regimes the reference pressure is 24 MPa. In Regime #1 the inlet temperature is 318.7ºC, heat flux – 789 kW/m^2 and mass flow rate – 987 kg/(m^{2}s). In Regime #2 these values: 352ºC, 884 kW/m^2 and 1500 kg/(m^{2}s) respectively. Both regimes correspond to group IV according to the classification (Kurganov et al., 2016) for deteriorated heat transfer. The characteristic axial temperature profile during upward motion contains peaks of wall temperature of significant width.

The results, obtained using proposed and adopted by IPP TMM method are compared with both experimental data and appropriate results obtained when applying FEM of the Pipe Flow module in COMSOL Multiphysics (see Figure 21).

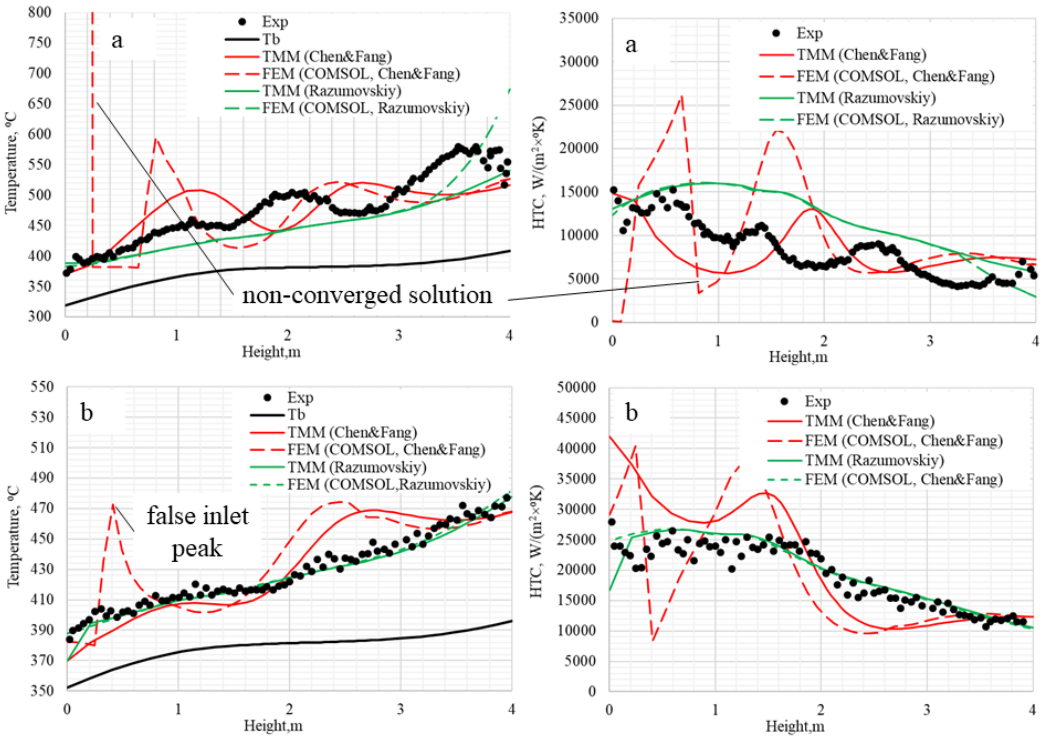

Figure 21. Results of calculations obtained by TMM in comparison to COMSOL FEM application, a – Regime #1, b – Regime #2

Using Chen&Fang correlation (4-6) for Regime #1 in COMSOL, a convergent solution could not be obtained in either the coupled or sequential approaches. The use of TMM makes it possible to obtain a convergent solution for both cases. The obtained results demonstrate the increased reliability of the TMM method for the selected regimes. In each of the application cases, the solution does not detect a false temperature peak, and the profile corresponds to the classification (Kurganov et al., 2016). Also, the TMM method stability with various combinations of applied boundary conditions is demonstrated in (Filonov et al., 2022). This feature is also one of the main advantages of TMM.

4.3 Application of the TMM method for regimes with HTD and correlation "robustness" map preparation

The adopted TMM method was successfully applied by IPP in the framework of ECC-SMART internal benchmarking of system codes organized by UNIPI. One of the main aims of these activities was the testing the "robustness" of correlations and applicability of the models and methods. The more detailed description of this benchmarking is described in more details in deliverable D3.2.

During this benchmarking, the following HTC correlations were implemented in TMM: Bishop, Mokry, Razumovskiy (Filonov et al., 2018), Deev, Yang (DHT) and Kurganov procedure (an original version that was built and tested on CO_2). As analysed experimental regimes the NTUU and Kirillov data described in deliverable D3.2 was used. The most illustrative cases for NTUU rod bundles data are combined in Figure 22-Figure 24.

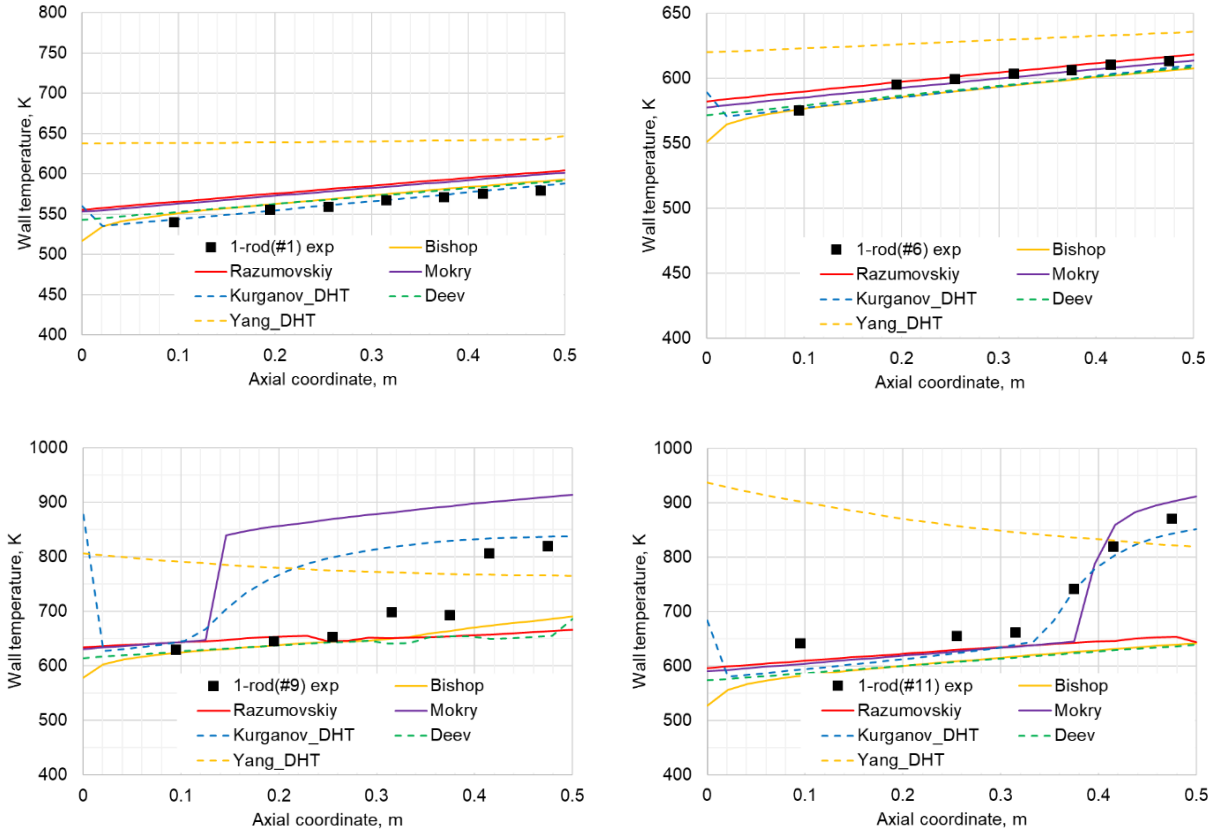

Figure 22. Calculation results by TMM for the selected cases (NTUU, 1-rod bundle)

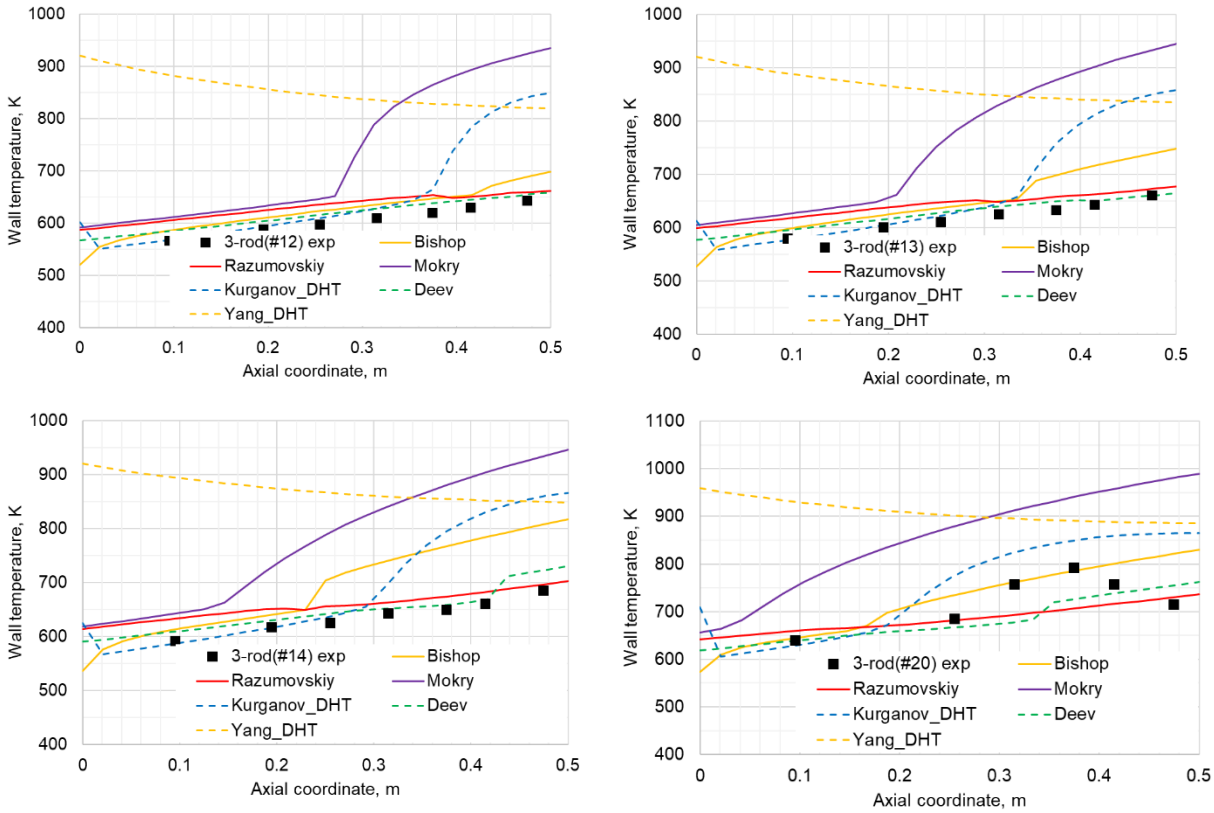

Figure 23. Calculation results by TMM for the selected cases (NTUU, 3-rod bundle)

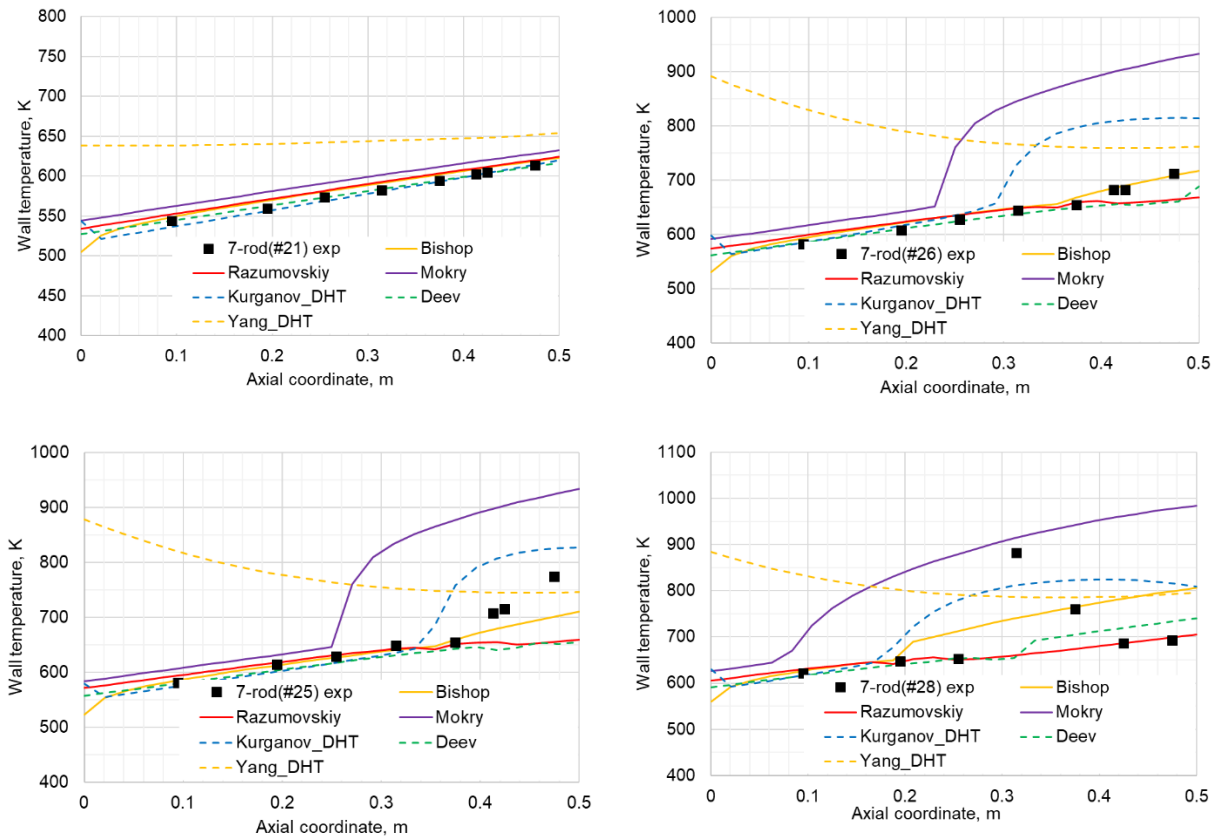

Figure 24. Calculation results by TMM for the selected cases (NTUU, 7-rod bundle)

According to results for 1-rod bundle (Figure 22), the satisfactory prediction of the axial wall temperature profile was obtained for regimes with "linear" heat transfer. But for cases with HTD (wall temperature peaks), predictive abilities were not so successful. The similar situation was captured for both "linear" and "deteriorated" heat transfer regimes in 3- and 7-rod bundles. And only some correlations were able to predict the presence of temperature peaks, but only qualitatively without quantitative agreement.

This situation drew IPP's attention to the issue of assessing the so-called "robustness" of correlations, i.e. assessment of their ability to predict wall temperature profile for various heat transfer regimes at supercritical coolant parameters. In this direction the Joint work of UNIPI, BME and IPP was conducted (Varju et al., 2024), where the abilities of two 1-dimensional codes (APROS and TMM) when implementing the chosen HTC correlations were examined.

In order to provide better understanding in question of choosing the HTC correlations for subsequent analyses, the whole set of known 59 correlations (Kassem et al., 2022) including one "procedure" for predicting regimes with HTD (Kurganov et al., 2018) was implemented in TMM. The "robustness" of each of the implemented correlations was tested on the full set of experimental data (described in deliverable D3.2) for supercritical water flow in the bare tubes and rod bundles.

According to the previous definition of "robustness", two sets of mappings for all the correlations were prepared: calculations are carried out "*a priori" or explicitly* (i.e., based on the known experimental wall temperature), as well as *implicitly* (i.e., using the TMM and evaluating independently the wall temperature) for each correlation. The calculation results for each correlation are visualized by separate sets of graphs for Nusselt numbers, HTC, wall temperature and temperature difference between wall and bulk, T_w - T_b, which compare experimental and

calculated values (see Varju et al., 2024). Such visualisation for the whole HTC correlations set could be named as “correlations robustness map”, which makes it possible to analyze and identify those correlations that have both a convergent solution and the smallest percentage of deviation of the predicted wall temperature from the experimental value.

This analysis turned out to be quite extensive, however, it was implemented due to the relatively high calculation speed and stability of the proposed TMM method. The idea of performed analysis was to identify a list of HTC correlations that have the best results in the "prediction" mode. According to the constructed “robustness map”, the best wall temperature prediction ability was obtained by the following correlations:

- Dyadyakin&Popov, Gorban, Deev, Bishop, Razumovskiy and Dittus&Boelter – for the Bare Tubes;
- Deev, Gorban, Bishop, Jackson-Hall, Kondratev, Krasnoshchyokov&Protopopov – for the Rod Bundles.

Chosen HTC correlations were applied by IPP in the framework of Joint work (Varju et al., 2024). Analysis included the same list of NTUU regimes for rod bundles in which HTD was observed during internal benchmarking activities (Figure 22 - Figure 24). Figure 25 shows appropriate results obtained using the HTC correlations chosen from “robustness maps”.

1-rod bundle (Regimes #9 and #11)

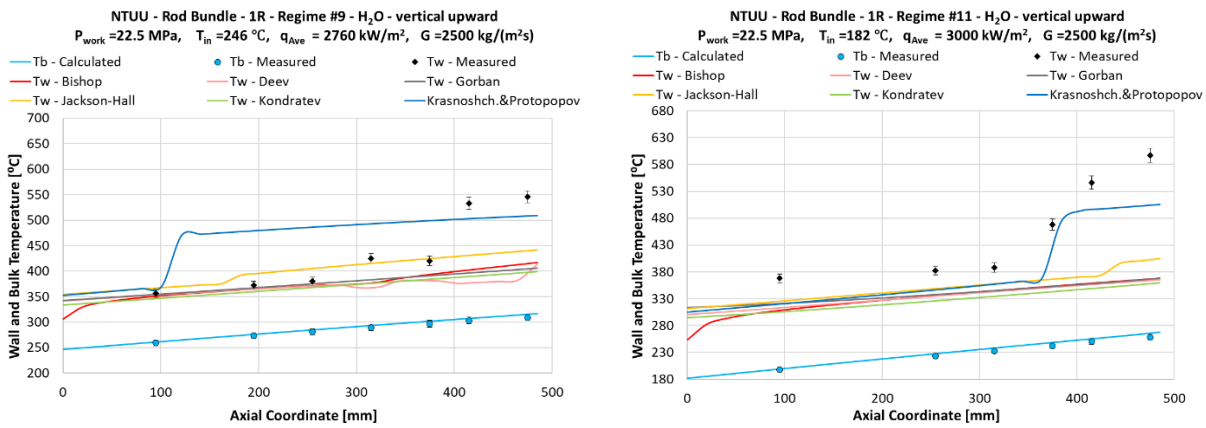

3-rod bundle (Regimes #14 and #20)

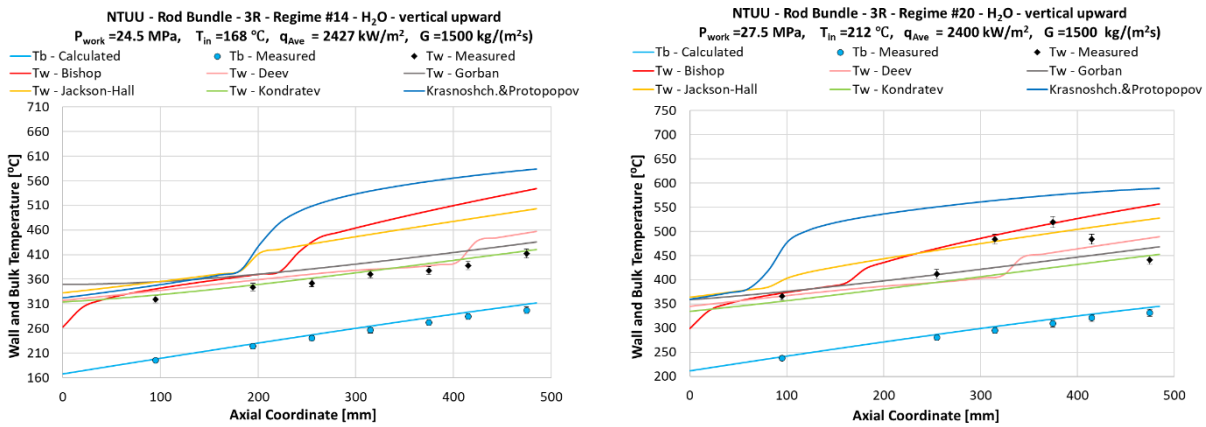

7-rod bundle (Regimes #25 and #28)

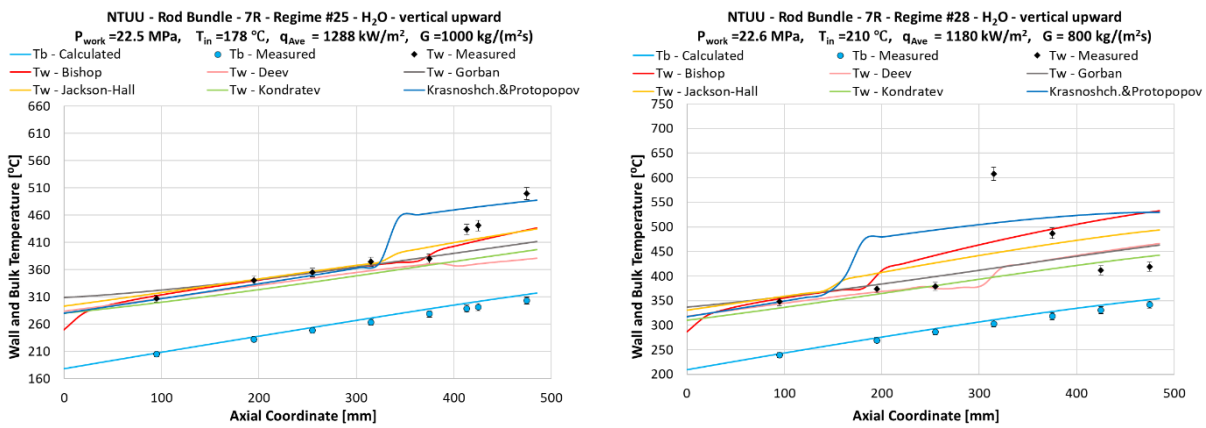

Figure 25. Calculation results obtained for HTD cases (NTUU, 1-, 3- and 7- rod bundles) using correlations chosen based on “robustness maps” analysis

According to Figure 25, the use of a set of correlations selected based on the "robustness maps" shows the better result in comparison with the initial analysis (Figure 22 - Figure 24). Namely, for all regimes the HTD is captured not only qualitatively, but also quantitative indicators (temperature peaks) are predicted with better accuracy. Nevertheless, the resulting picture cannot be called

completely satisfactory, because the position of the wall temperature peaks is still predicted quite poorly.

4.4 Non-linear differential method for predicting HTC and PLF

In further work IPP examined the issues of constructing a special function (Filonov et al., 2024), which, based on differential equations for the functions of energy dissipation and heat transfer, would be capable to predict the HTD regimes.

Heat transfer deterioration in the supercritical region is a multifactorial problem, which is determined not only by the extremely nonlinear behavior of thermophysical properties, but also by nonlinear turbulent transport. Modern CFD packages can be used for such purposes, which only in limited cases can represent both the qualitative and quantitative picture (see deliverable D3.5). Also, the use of system analysis definitely has a significant advantage in the relative simplicity and calculation speed, where a number of parametric calculations can be performed to form the basis of an optimization mesh.

This section propose the differential method, based on the "narrow channel" model, which contains the advantages of one-dimensional thermal-hydraulics and CFD methods, as follows:

- Implementation simplicity and minimal calculation requirements (1D).
- Possibility to take into account physical features in the heated wall (CFD), which include the significant influence of the shear stress profile (He et al., 2016; Kurganov et al., 1993).
- Provides the ability to operate with different kinds of functional dependencies defined by both local (CFD) and global flow characteristics, such as similarity criteria (1D).
- Allows to consider the non-uniformity of the velocity and temperature field, including the turbulent flow structure (CFD).
- Characterized by unification of the numerical implementation, or rather, the iterative procedure (Filonov et al., 2022), which is a guarantee of effective organization of multiphysics calculations.

4.4.1 Method description

The hydraulic resistance and heat transfer coefficient functions, which are determined through the similarity criteria, in the first approximation could be interpreted as transverse exchange functions. That is, according to strict theoretical concepts, they are defined in the form of diffuse components that depend at least on the radial gradient of longitudinal velocity and temperature. So, starting from the one-dimensional formulation, the external exchange functions can be represented as (4-9). It should be noted, that the strict theoretical transition is carried out backwards, i.e. from diffusion terms to algebraic relations by averaging on perimeter and cross section.

$$\begin{aligned} \xi\rho w|w| &\rightarrow \int \frac{\partial}{\partial r}\left[\mu\frac{\partial w_x}{\partial r}+\tau_t\right]dr \\ \phi(T,T_{wall}) &\rightarrow \int \frac{1}{r}\frac{\partial}{\partial r}\left[\lambda\frac{\partial T}{\partial r}+q_t\right]dr \end{aligned} \tag{4-9}$$

The term responsible for the dissipation of flow energy into the thermal energy is governed by multiplying the stresses by the flow velocity in the longitudinal direction. The turbulent heat flux

and stresses are functions of the flow, as adopted in the RANS approach, and are generally evaluated by correlations of velocity and temperature pulsations. The introduction of a differential formulation for the determination of the dissipation and heat transfer intensity functions requires the calculation of the radial distribution of the longitudinal velocity component, which leads to the need to introduce the radial component into the system of one-dimensional equations:

$$\begin{cases} \frac{\partial}{\partial r}\left[r \cdot G_r\right] + \frac{\partial}{\partial x}\left[r \cdot G_x\right] = 0 \\ \frac{\partial}{\partial r}\left[\frac{r \cdot G_r G_x}{\rho}\right] + \frac{\partial}{\partial x}\left[\frac{r \cdot G_x G_x}{\rho}\right] = -r\underbrace{\frac{\partial p}{\partial x}}_{\text{Axial gradient}} - r \cdot g\left(\rho - \rho_0\right) n_x \underbrace{+ T_p}_{\text{Diffuse term}} \\ \frac{\partial}{\partial r}\left[r \cdot G_r h\right] + \frac{\partial}{\partial x}\left[r \cdot G_x h\right] = -r \cdot g\left(\rho - \frac{\rho_0}{\rho}\right) \cdot \left(G_x n_x + G_r n_r\right) \underbrace{+ \gamma T_T}_{\text{Diffuse term}} + \frac{\partial}{\partial x}\left[r \cdot \chi \frac{\partial h}{\partial x}\right] \underbrace{+ T_F}_{\text{Diffuse term}} \end{cases} \tag{4-10}$$

Where the T_p, T_T, T_F - are the diffusion terms, described in detail in deliverable D3.5.

Similar to the approach (Filonov et al., 2022) it is assumed that the flow characteristics are the longitudinal mass velocity ρwx=Gx, transverse mass velocity ρwr=Gr, and h - enthalpy of the supercritical fluid flow. In order to operate with a homogeneous system in the sense of the adopted variables, the modified Newton's laws for shear stresses, as well as Fourier's law were introduced, which in the context of this formulation are defined as follows:

$$\tau = \frac{\mu_{ef}}{\rho}\frac{\partial G_x}{\partial r} - \delta\tau; q = \frac{\lambda_{ef}}{c_p}\frac{\partial h}{\partial r} \tag{4-11}$$

There is doubtless in the validity of (4-11) for isothermal flow, but for non-isothermal flow cases the exactly this form is also often found in the literature, at least for the energy equation (Valueva, 2012; Popov, 1977). Advantage of the form (4-11)for the thermal energy equation is in following. The point is that in the case of no exchange of mass, momentum and energy through the wall (injection problem), the enthalpy function is always monotonically increasing or decreasing (heating/cooling), unlike the temperature, which has an extremum in the case of deteriorated heat transfer, and therefore the temperature gradients at this point should be calculated more accurately. On this basis the above mentioned form for determining the contacting stresses is adopted, which, according to the idea, would make it "more simply" to calculate the velocity field having an inflection point, which is relevant in the case of the so-called M-shaped radial profiles (Kiss et al., 2017). It should be also noted that the strict equivalence of (4-11) with the classical form is achieved only when the radial gradients of thermophysical properties are insignificant. The correction is purely mathematical and is calculated explicitly, i.e., it does not depend on the flow parameters at a given iteration.

The more detailed description of determination the turbulent heat transfer characteristics adopted in Differential procedure was given in deliverable D3.5 in the framework of the Eddy viscosity turbulence model modification proposed by IPP.

4.4.2 Numerical solution

The system (4-10) is nonlinear and none enclosed with respect to the variables. To construct the solution, it is convenient to assume that the longitudinal pressure gradient is an external parameter. For its determining the TMM module (see section 4.2) is used.

Using the concept of "basic" and "correcting" value (see section 4.2.1) and using the linearization rules formed in (Filonov et al., 2022), it is possible to present the solution at a known pressure gradient in the following form:

$$\begin{cases} G_r \approx (G_r)_0^{base} + \sum_{i=1}^{n} k_{dyn} (G_r)_i^{cor} \\ G_x \approx (G_x)_0^{base} + \sum_{i=1}^{n} k_{dyn} (G_x)_i^{cor} \\ h \approx h_0^{base} + \sum_{i=1}^{n} k_{dyn} h_i^{cor} \end{cases} \quad (4\text{-}12)$$

Where n – is a number of approximations, k_{dyn} – decomposition factor (effective correction factor), index «0» - initial approximation.

The linear form of (4-10) at the current iteration is solved using FEM, in which the form function is taken as first or second order (4-13) in the coupled formulation of the "mass velocity-enthalpy field" type.

$$\Pi^{cor}(r,x) = \forall_{(r,z)\in E_m} \left[\begin{array}{l} 1: a_{i1} r + a_{i2} x + a_{i3} rx + a_{i4} \\ 2: a_{i1} r + a_{i2} x + a_{i3} r^2 + a_{i4} x^2 + a_{i5} rx + a_{i6} \end{array} \right. \quad (4\text{-}13)$$

The computational mesh implemented for this method is regular with the power law support, with non-uniform discretization, both in the radial (near the wall/axis) and in the axial direction (e.g., when using Neumann conditions at the inlet and outlet boundaries). The general view of mesh is shown in Figure 26. It is based on rectangular elements of the 1st or 2nd order (specified during initialization). Defining parameters for mesh generation are: the number of elements in the radial and axial directions, the method and coefficients of element densification, along with the parameter responsible for the approximation order. The current version of the procedure uses a structured, irregular rectangular mesh with three conventionally distinguished groups of anisotropy.

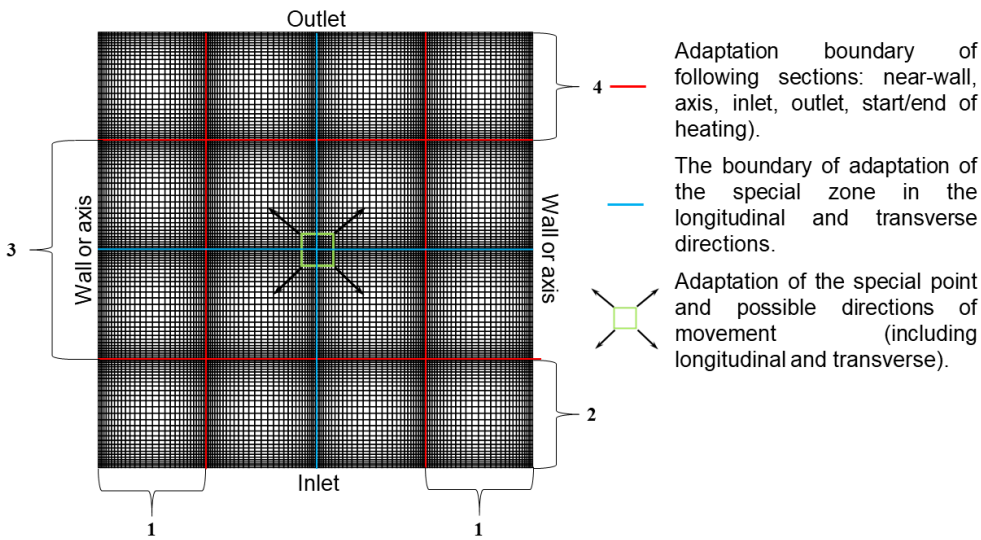

Figure 26. General view of the computational mesh

Adaptation here is possible both directly at the boundary and in the places of connection of the conditional stabilization and heating zones (transversely) and of the boundary region with the core

flow. This type of adaptation is necessary to dispose the possible oscillations in the case of stepwise changes of the heat flux. The second and third types of adaptation refer to the so-called special zones in the longitudinal and transverse direction, including a special point (e.g., at the wall at the place of minimum effective viscosity). It should be noted that this is rather limited in application, but the easiest to implementation method. Additional features such as parameter or isoline adaptation will be introduced in further studies.

To define the pressure gradient dp/dx, two methods are provided. The first is based on the mass velocity conservation condition along the channel and can be represented as function (4-14). The proposed dependence characterizes the deviation of the current pressure value at a point from the value specified at the inlet boundary.

$$p(x)_{new} = p(x)_{old} + \frac{C}{\rho}\left[\left(\frac{1}{r_2^2 - r_1^2}\right)\int_{r_1}^{r_2} rG_x dr - G_x^{in}\right]\left|\left(\frac{1}{r_2^2 - r_1^2}\right)\int_{r_1}^{r_2} rG_x dr - G_x^{in}\right| \quad (4\text{-}14)$$

Where C is a constant that characterizes the rate of convergence of the pressure field and mass velocity.

The second method is implemented as an auxiliary procedure for the calculation of one-dimensional thermal hydraulics using TMM (Figure 27).

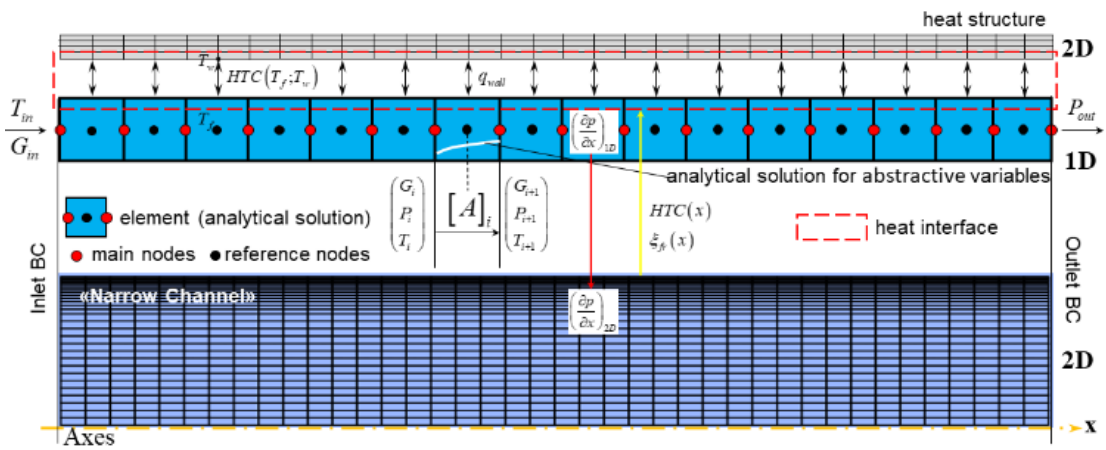

Figure 27. The scheme of coupling the 2D Differential procedure ("Narrow channel") with the 1D TMM method

The idea of such coupling is in use the 2D differential "narrow channel" model to calculate the heat transfer and hydraulic resistance coefficients, which are input coordinate functions for the one-dimensional calculation. Based on the resulting pressure distribution, the one-dimensional pressure gradient is calculated as a function of the longitudinal coordinate, which is the input to a new iteration of the "narrow channel" model. The coupling functions are formed as follows:

$$\mathrm{HTC}(x)=\frac{q(x)d_T}{\lambda}\left[T(2R_0,x)-\underbrace{\frac{2}{G_x^{in}\cdot R_0^2}\int_0^{R_0}G(r,x)T(r,x)rdr}_{T_f}\right]^{-1} \tag{4-15}$$

$$\xi_{fr}(x)=-8\tau_w\rho_f\left(G_x^{in}\right)^{-2} \tag{4-16}$$

$$\left(\frac{dp}{dx}\right)_{1D}=\left(\frac{dp}{dx}+\rho_{in}n_x g\right)_{2D} \tag{4-17}$$

Dependence (4-16) defines the friction resistance coefficient, whereas (4-17) - the differences in the formalization of pressure gradients in 1D and 2D approximations.

The calculation procedure provides the possibility of estimating the thermal acceleration resistance coefficient and the buoyancy, which can be obtained from (4-18).

$$\begin{aligned}\xi_{ac}(x)&=\frac{4d_h}{\left(G_x^{in}\right)^2}\frac{d}{dx}\left[\frac{2}{R_0^2}\int_0^{R_0}\frac{G(r,x)^2}{\rho(r,x)}rdr\right]\\ \xi_g(x)&=\frac{4g\cdot n_x}{\left(G_x^{in}\right)^2}\left[\frac{2}{R_0^2}\int_0^{R_0}\left(\rho(r,x)-\rho_{in}\right)rdr\right]\end{aligned} \tag{4-18}$$

4.4.3 Application of differential procedure for calculating regimes with HTD

A demonstration of the application of the proposed differential procedure for calculating regimes with deterioration in heat transfer is the most indicative. The NTUU experimental cases obtained on 3-rod and 7-rod bundles are chosen for this purpose. For each rod bundle configuration, both cases with normal and deteriorated heat transfer are considered. The main operating parameters of the selected cases are presented in Table 2.

Table 2. The main operating parameters for chosen NTUU regimes

Test section	Pref, [MPa]	G, kg/(m2s)	Tin,[ºC]	q, [kW/m2]
3R(N)	24.5	1500	168	2216
3R(D)	27.5	1500	212	2400
7R(N)	24.5	800	184	959
7R(D)	27.5	800	210	1180
N – normal heat transfer (NHT), D – deteriorated heat transfer				

In calculations, the “narrow channel” procedure is coupled with the 1D TMM method. The interaction is organized on the basis of system (4-15)-(4-17) as follows. The heat flux value is specified for the TMM, and in the proposed two-dimensional model, a boundary condition of the first kind is used in the form of axial wall temperature distribution. The temperature of the TMM wall is calculated using the balance flow temperature, and in the “narrow channel” model using

relation (4-15). In this example, the solid wall is not considered, although the correct prediction of the regime is apparently influenced by the specifics of accounting for heating. The unevenness of the heat flux, which was estimated based on the reduction of the test section balances (when processing experimental data), is taken into account during calculations in the TMM in the form of a first-order interpolation function. For the narrow channel model, the average value of the heat flux is used when calculating the heat transfer coefficient.
Since TMM makes it possible to use the characteristic diameter individually for each equation and explicitly specify the heat transfer and friction area, it is not difficult to represent the rod bundle in the channel approximation using the appropriate geometric data (see deliverable D3.2). At the same time, the current setup is, strictly speaking, built for a channel with a circular cross-section. Although the current implementation attempts to account for individual thermal and hydraulic perimeters, it still requires more rigorous justification and testing. Thus, the issue of choosing the characteristic diameter remains relevant, and in general affects the result, as shown below.

The computational domain for the one-dimensional approximation is divided into 40 nodes. The two-dimensional procedure has a computational mesh of 50 nodes in the radial direction and 100 in the axial direction. The computational mesh is refined near the wall with a growth factor of 1.2 ÷1.25, so that y+~1.0. Since the mass velocity profile is assumed to be uniform, the computational mesh at the inlet and outlet is refined with a growth rate of 1.025 to suppress oscillations on the first iterations. Functions of form (4-13) are applied for each of the first order parameters.

TMM boundary conditions are applied to the channel inlet (pressure, mass flow rate, temperature). The initial pressure gradient is 100 Pa, and the wall temperature is Tin+5ºC.

The comparison of obtained results both with the experimental data (deliverable D3.2), and with the profiles obtained using the correlations of Mokry, Bishop and Deev is performed. Also, for regimes with deteriorated heat transfer, an additional comparison with CFD (Dubyk et al., 2022) results using the SST turbulence model in the low-Re approximation (y+ <1.0) is performed.

Figure 28 shows the axial temperature distribution for normal heat transfer conditions obtained with application the various reference diameters in the narrow channel (NC) model. Several options for choosing a characteristic diameter were considered: hydraulic, thermal, as well as their linear combination. When using the hydraulic diameter for TMM+NC, the estimated temperature is always lower than in the experiment, and when using the thermal diameter, it is higher. Through numerous tests for a given geometric configuration, it was noted that good agreement with experiment is achieved when the reference diameter for a narrow channel is estimated using the following linear combination:

$$D_{ref} = \frac{n-1}{n} D_h + \frac{1}{n} D_{heat} \qquad (4\text{-}19)$$

Where n – the number of rods in the bundle.

The equation (4-19) cannot claim to be universal for this model, but at least it is unambiguously applicable for a bare tube and most likely for an annular channel. In addition, (4-19) turned out to be applicable for calculating HTD regimes (Figure 29).

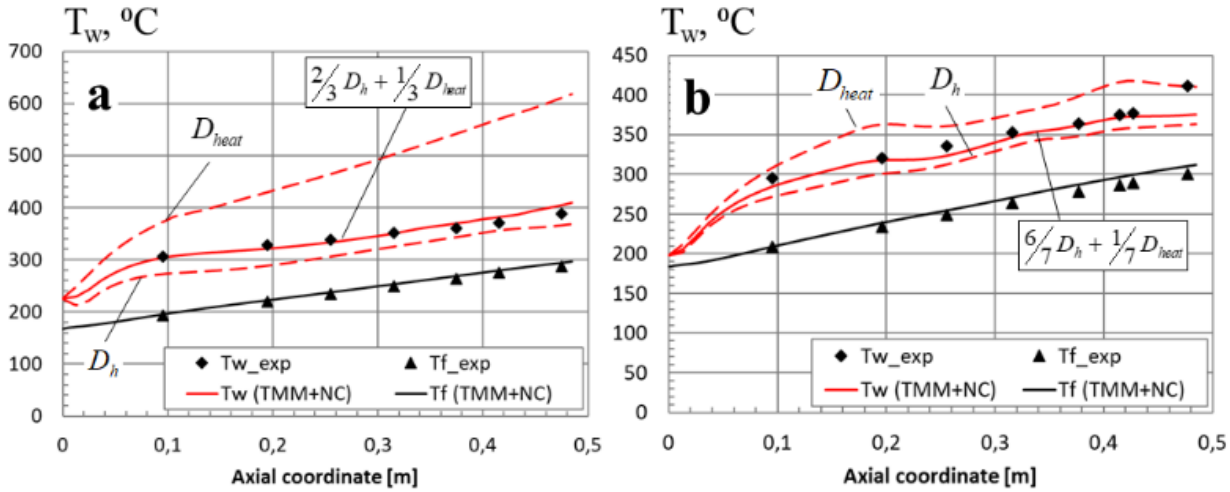

Figure 28. Axial distribution of bulk flow and wall temperatures for NHT regimes: a – 3R(N), b – 7R(N)

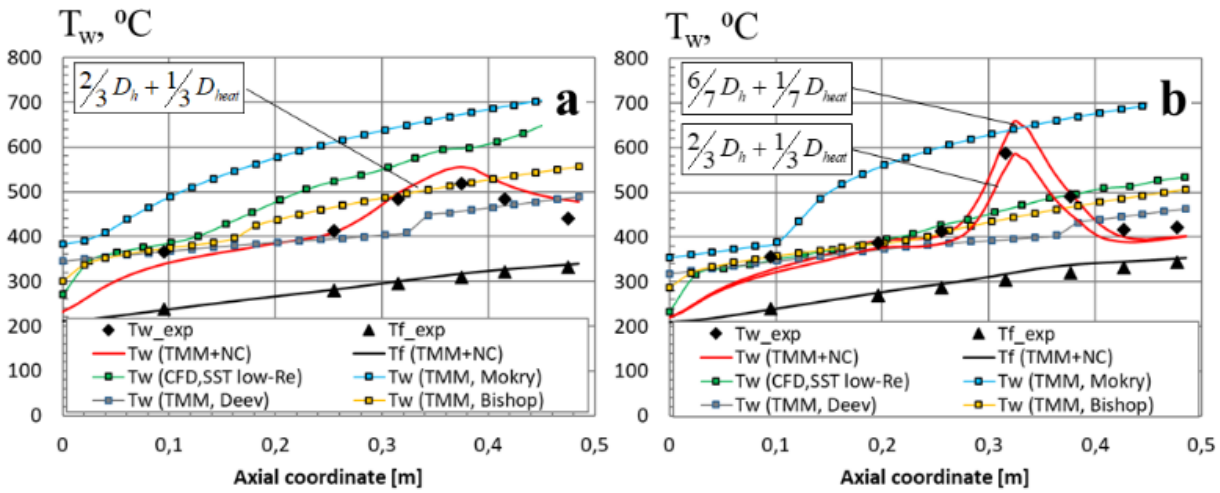

Figure 29. Axial distribution of bulk flow and wall temperatures for regimes with HTD: a – 3R(D), b – 7R(D)

The results obtained are encouraging, since using the proposed TMM+NC approach, the magnitudes of the temperature peaks, as well as their locations are predicted with sufficient accuracy. Also, the physical features in the form of a decrease in turbulent transport (Figure 30) are captured. At the same time, the considered correlations, as well as CFD (SST, Low-Re) with the standard turbulence model available in commercial packages (results obtained in ANSYS CFX) do not predict the experimental temperature peak.

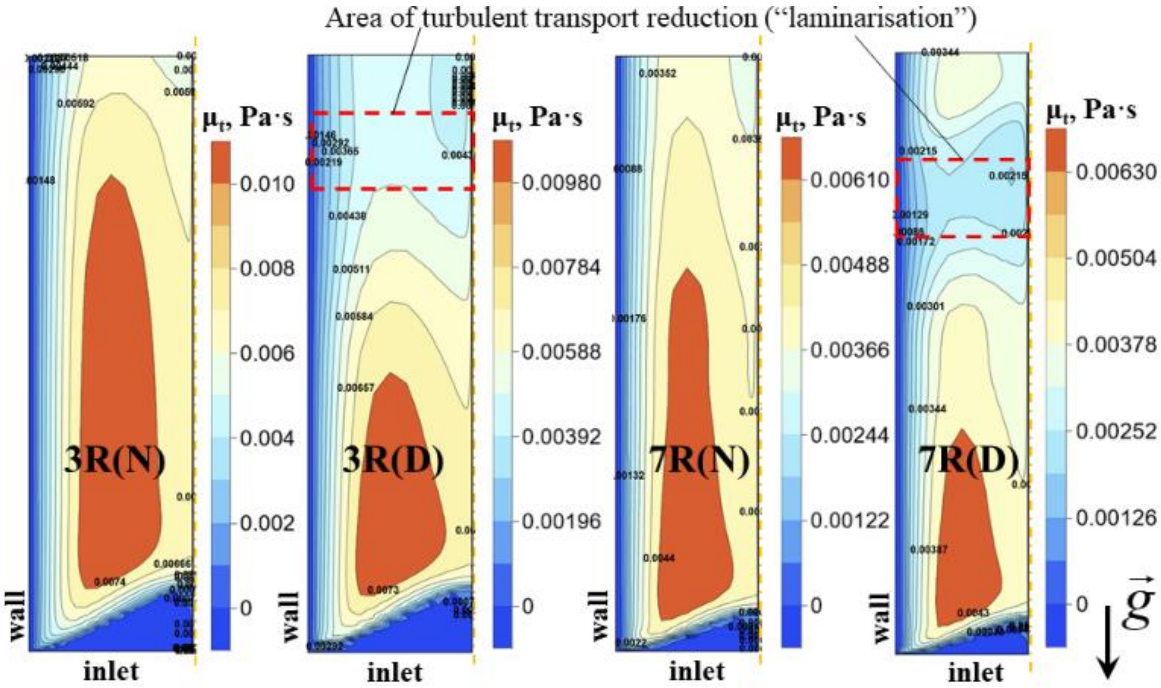

Figure 30. The calculated values of turbulent viscosity obtained for each regime (reference diameters calculated according to (4-19))

It is important to note that in each of the considered calculation cases, the flow temperature in the TMM coincided with the mass-average flow temperature, calculated in the narrow channel model by integrating over the radius.

Comparison of the experimental total pressure drops with the obtained in TMM+NC is provided in Table 3. The higher values of pressure drops can be explained by the axisymmetric arrangement of the inlet section due to the use of a uniform mass velocity, which leads to the waste of flow energy on profile restructuring. These features will also be taken into account in the future.

Table 3. The comparison of total pressure drop values

	3R(N)	**3R(D)**	**7R(N)**	**7R(D)**
ΔPexp, Pa	6920	7350	3030	3360
dPTMM+NC, Pa	7578	7229	5446	5287
1dPTMM, Pa	6096	6321	2481	2740
1- the heat transfer and frictional resistance coefficients were calculated using Razumovskiy's correlations (IAEA-TECDOC-1900; Filonov et al., 2022)				

According to obtained results, the proposed differential procedure for estimating heat transfer and hydraulic resistance coefficients is a good alternative to empirical correlations, but still requires testing for various geometric characteristics and operating parameters.

4.5 Concluding remarks

Performed in IPP work on adaptation of transfer matrix method (TMM) for the analysis of non-linear thermal hydraulic processes has opened up new possibilities in the calculations and analysis of the flow of media under supercritical parameters. The demonstrated stability and computational efficiency of the adopted TMM method allowed IPP to conduct a computational analysis for the full set of experimental regimes using 59 different HTC correlations. Based on this analysis, the "correlation robustness" maps were generated, which allowed IPP to identify those correlations that have the best capabilities for predicting axial temperature profiles. Nevertheless, even after application the chosen correlations, the resulting picture could not be called completely satisfactory, because in regimes with HTD the position of the wall temperature peaks was still predicted quite poorly.

Then, the creation of special non-linear differential method for prediction of HTC and PLF based on “narrow channel” model was proposed. This approach was implemented as a special function, which, based on differential equations for the functions of energy dissipation and heat transfer, is capable of predicting deteriorated heat transfer regimes. The proposed model was used as a differential procedure for calculating the heat transfer and friction resistance coefficients together with the one-dimensional TMM approximation. Heat transfer regimes for NTUU 3- and 7-rod bundles were considered, among which two related to normal heat transfer, and another two - to deteriorated heat transfer. The results obtained are encouraging, since using the proposed TMM+NC approach for HTD regimes, the magnitudes of the temperature peaks, as well as their locations could be predicted with sufficient accuracy.

5 Subchannel Analysis for Supercritical Flows - CNL

One of the critical components in a nuclear reactor design is the fuel bundle or assembly, which contains the nuclear fuel in the reactor. Therefore, the fuel assembly must be designed so that all the heat generated within the fuel rod is removed properly to minimize the possibility of material failure. Subchannel analysis is a common approach used to design or study bundle modifications. This approach models the flow in the fuel bundle with multiple parallel flow paths called subchannels. Each subchannel is bounded by the element walls and the imaginary boundaries along element centre-to-centre lines and the pressure tube wall (for outer subchannels). Within each subchannel, the flow is considered one-dimensional (predominantly axial flow), and the lateral exchange of mass, momentum, and energy between interconnected subchannels is modelled with a simplified lateral momentum and energy equation system, along with constitutive relations. This lateral exchange, also called mixing, is a vital component of the flow distribution.

The use of computational tools to design nuclear reactors must follow software quality assurance standards. It is important to estimate the uncertainties of the code predictions for intended applications. Validation exercises comparing code predictions against experimental data are used for this purpose. Statistical parameters such as bias (or average difference), standard deviation, and root mean square (RMS) are used to quantify the uncertainties.

Throughout the development of SCWR concepts, multiple thermal-hydraulics experimental campaigns have been carried out worldwide to shed light on the thermal hydraulics characteristics of supercritical water and generate data for code validation. Until now, most of these experiments have focused on heat transfer and hydraulic resistance. In addition, multiple international benchmarking efforts have been organized to assess computational tools such as subchannel codes and computational fluid dynamics codes.

However, the effect of surface finishing has not been considered. It is known that supercritical water is a corrosive environment, and oxide deposits in the fuel cladding impact the designed flow and temperature distribution of the fuel assembly. The reason for these changes is the additional thermal layer caused by the deposits (crud) which directly affects the surface's heat transfer and roughness.

5.1 Subchannel code ASSERT-PV

ASSERT-PV (Nava Dominguez et al. 2014) is a Canadian subchannel code developed and qualified for predictions of subchannel flow, enthalpy and phase distributions, heat transfer, and fuel cladding temperatures in horizontal fuel channels of pressurized heavy water reactors (PHWRs). The code has been designed to be general enough to accommodate other geometries and orientations. These include simple geometries of a few subchannels and bundles or assemblies relevant to PHWR, pressurized water reactors, and boiling water reactor designs in vertical and horizontal orientations. The code can accommodate a range of fluids, including single- and two-phase heavy water and light water, various Freons, and air-water mixtures.

ASSERT-PV is based on ASSERT-IV (Carver et al. 1990), which in turn originated from the COBRA-IV computer program (Wheeler et. Al. 1976). ASSERT-PV has been enhanced to meet the specific requirements for the thermal-hydraulic analysis of two-phase flow in the horizontally oriented PHWR fuel channels. The ASSERT-PV version for SCWR analysis is V3R2m2, also

referred to as ASSERT-PV 3.2-SC in this paper. It was developed to model flow and heat transfer in subchannels of fuel bundles under supercritical pressure conditions. This interim version can accommodate supercritical flows, but not the transition between supercritical and subcritical flows when the system pressure varies across the critical point during a transient. This is considered sufficient since phase transition and transients are not required in a subchannel analysis at this stage of conceptual development of the Canadian SCW-SMR. The subchannel code ASSERT-PV 3.2-SC is an extended ASSERT-PV version specifically developed for modeling subchannel flow and heat transfer in fuel bundles under steady state supercritical conditions.

Using three available experimental data of test section operating under supercritical conditions, ASSERT-PV was subjected to a validation exercise to quantify the uncertainty prediction of the subchannel code ASSERT-PV. The focus of this validation was on hydraulic resistance, specifically pressure drop.

5.2 Experiments

Three datasets were used for the validation exercise: 1) the 1rod and 7rod wire-wrapped channels from NTUU (Razumovsky et al. 2008, Razumovskiy et al. 2016) , 2) the 2×2 wire-wrapped fuel bundle from XJTU (Wang et al. 2014) , and 3) the single pipe cooled with supercritical CO2 from CNL (previously Atomic Energy of Canada Limited) (Khartabil, 2005). The uncertainties associated with these experiments are listed in Table 4.

Figure 1 depicts the subchannel discretization of the (a) NTUU 3-rod bundle experiments and b) the 2x2 fuel subassembly from the XJTU dataset.

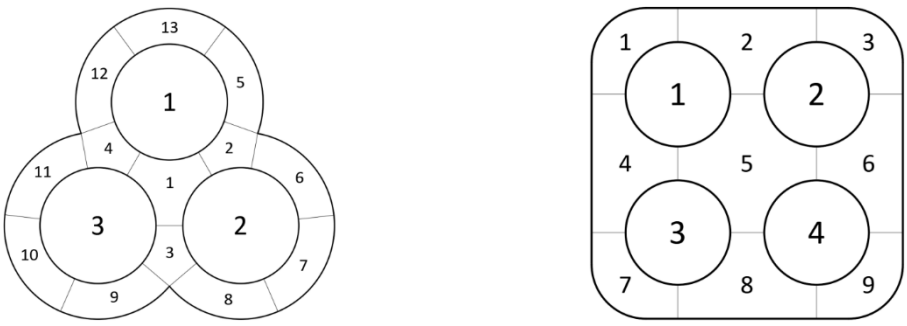

(a) (b)

Figure 31 ASSERT-PV 3.2-SC subchannel discretizations for (a) the NTUU 3-rod assembly and (b) the 2×2 XJTU cases

To assess the effect of the roughness of the cladding material on the ASSERT-PV predictions, several sensitivity analyses were performed and discussed in the following paragraphs.

ASSERT-PV 3.2-SC predicted pressure drops for 777 tests. The overall code bias is +3.4%, with a variation in the bias of 14.5%. The RMS of the prediction errors is 14.9%. Generally, ASSERT-PV 3.2-SC overpredicted the channel pressure drops of the supercritical tests for various test sections and various fluids. The range of code bias is from +0.5% to +16.1%, and the range of RMS is from 7.7% to 27.5%. These results are summarized in Table 5. To assess the impact of

various parameters, sensitivity analyses were performed. These are summarized in Table 6 and Table 7.

The results are discussed as follows:

The ASSERT simulation results show that the prediction error of pressure drops for tube tests increases as the ratio of heat-flux to mass flux (q/G) increases. However, the trend is not true for tests with heated subassemblies.

For the smooth tube, both the Colebrook-White correlation (with surface roughness of zero) and the Blasius correlation overestimate the frictional pressure drops, with the Blasius correlation providing predictions with a small degree of over-prediction. For the rough 3-rod bundle, the selection from the Colebrook-White (White, 2011) correlation and its variants had negligible effects on the simulation results.

The options of the mixing models have a small effect on the calculations of the pressure drop in a rod bundle or fuel assembly.

A sensitivity study indicated that the number of axial nodes used in the ASSERTPV 3.2-SC models is sufficient to converge to the calculation results. The uncertainties in the boundary conditions have small effects on the validation results.

The friction coefficient models in the current version of ASSERT-PV 3.2-SC are valid for only isothermal flow. The models overpredict the frictional pressure drops at supercritical conditions. This is due to the abrupt fluid properties change in the bulk flow and near the heated wall when the fluid temperature approaches the pseudo-critical point. To take into account the characteristics of the frictional pressure losses at supercritical pressures, a simple approach is to apply correction factors to the friction coefficients for isothermal flows (Nava Dominguez, 2020). Those correction factors reflect the difference of fluid properties at the bulk and wall temperatures. To improve the accuracy of ASSERT-PV 3.2-SC in the predictions of pressure drops under supercritical conditions, it is recommended that friction correction factors be implemented in ASSERT-PV 3.2-SC (Nava Dominguez, 2020).

Chyba! Nenalezen zdroj odkazů. shows that the most significant deviation from the base case occurs when the Blasius friction factor equation is used instead of the Colebrook-White correlation.

Table 4. Uncertainties of measured and calculated parameters

Parameter	Uncertainty
NTUU	
Inlet pressure	±0.9%
Current	±0.5%
Voltage	±0.2%
Pressure drop	±2.0%
Mass flow rate	±2.3%

Parameter	Uncertainty
Water inlet/outlet temperature	±2.34%
Wall temperature	±3.21%
Calculated Parameters	
Heat flux	±3.5%
Heat transfer coefficient	±12.7%
Heat loss	≤2.4%
XJTU	
Pressure (MPa)	± 0.44%
Pressure drop (kPa)	±0.52%
Electrically heated power (kW)	±6.25%
Mass flow rate (kg/s)	±1.02%
Fluid temperature (°C)	±0.4%
Wall temperature (°C)	±0.16%
Heat transfer coefficient (kW/m2K)	±8.83%
AECL	
Test-section power (kW)	±0.5%
Outlet pressure (MPa)	±0.2%
Local pressure drops	±0.8% at ΔP = 30 KPa ±5.0% at at ΔP = 5 KPa
Temperatures	±0.3°C within 0 — 100°C ±2.2°C beyond 100°C
Mass flow-rates	±0.9% at 155 g/s (G=3084 kg/m2s) ±8.2% at 46 g/s (G=915 kg/m2s)

Table 5. Code bias and RMS in the ASSERT predictions of pressure drops

Experiment	Test section	Fluid	No. of tests	Code bias %	Variation %	RMS %
NTUU	Tube	H2O	17	+7.9	5.7	9.8
	1-rod channel	H2O	11	+7.1	13.9	15.6
	3-rod channel	H2O	9	+6.3	4.5	7.7
XJTU	2×2 rod channel	H2O	610	+0.5	10.7	10.7
AECL	Tube	CO2	130	+16.1	22.3	27.5
Overall			777	+3.4	14.5	14.9

Table 6. Results of sensitivity analysis using NTUU tube tests

Parameter	Variation	Bias (%)	Variation (%)	RMS (%)
Friction factor correlation	Colebrook-White (NFRIC=2) and absolute roughness of 0.0 m	+7.9	5.7	9.8
	Blasius * (NFRIC=0)	+5.2	5.6	7.6
Axial nodes	120 nodes (doubled)	+7.9	5.7	9.8
	60 nodes (base case)	+7.9	5.7	9.8
	30 nodes (halved)	+7.9	5.7	9.8
Boundary conditions	60 nodes (base case)	+7.9	5.7	9.8
	Pressure increased by 0.2%	+7.9	5.7	9.7
	Pressure decreased by 0.2%	+8.0	5.7	9.9
	Inlet temp. increased by 2.2°C	+9.8	6.5	11.7
	Inlet temp. decreased 2.2°C	+6.4	5.3	8.3
	Mass flux increased by 2.3%	+10.4	5.8	11.9
	Mass flux decreased by 2.3%	+5.3	5.7	7.8
	Heat flux increased by 2.4%	+8.8	6.1	10.7
	Heat flux decreased by 2.4%	+7.1	5.3	8.9

* The constants in the Blasius correlation are a=0.316, b=−0.25, and c=0.0.

Table 7. Results of sensitivity analysis using NTUU 3-rod tests

Parameter	Value Changed	Bias (%)	Variation (%)	RMS (%)
Friction factor correlation (NFRIC)	Selander (Selander, 1978) (NFRIC=1)	+6.4	4.5	7.8
	Colebrook-White (White, 2011) (NFRIC=2)	+6.3	4.5	7.7
	Chen (Groeneveld and Leung, 1997) (NFRIC=3)	+6.4	4.5	7.9
	Miller (Miller, 1990) (NFRIC=4)	+6.5	4.5	7.9

Mixing model (NSPMIX)	Rogers & Tahir (Rogers and Tahir, 1975) (NSPMIX=1)	+7.2	4.6	8.6
	Rehme (Rehme, 1992) (NSPMIX=2)	+6.3	4.5	7.7
Surface roughness	Roughness decreased from 1.5´10−6 m to 1.0´10−6 m	+4.7	4.2	6.3
	Roughness = 1.5´10−6 m	+6.3	4.5	7.7
	Roughness increased from 1.5´10−6 m to 2.0´10−6 m	+7.8	4.8	9.1
Contraction term coefficient in Idelchik formula (Idelchick, 1994)	GBCb(1) decreased from 0.3 to 0.2	+5.9	4.4	7.3
	GBC(1) = 0.3	+6.3	4.5	7.7
	GBC(1) increased from 0.3 to 0.4	+6.7	4.6	8.1

[b]GBC: Coefficient of contraction term in Idelchik's thick-edged orifice formula (Idelchik, 1994).

5.3 Concluding remarks

The validation exercise presented in the previous subsection shed light on the hydraulic resistance of diabatic flows at supercritical conditions. A correction factor is needed to partially consider the effect of the radial distribution of the flow. These correction factors have been implemented in a new interim version of ASSERT-PV SC. Preliminary results show that ASSERT-PV SC predictions improve after applying a friction correction factor, especially for flows near the critical, or pseudo critical point.

This validation exercise is the base platform for evaluating the improvement of the subchannel code ASSERT-PV SC.

6 References:

McFadden J H, Narum R E, Peterson C Eet al. RETRAN-02: A program for transient thermal-hydraulic analysis of complex fluid flow systems: Volume 1, Theory and numerics (Revision 4)[R]. Palo Alto, CA (USA): Electric Power Research Institute, 1988.

Andreani, M., Bittermann, D., Marsault, Ph., Antoni, O., Keresztúri, A., Schlagenhaufer, M., Manera, A., Seppäla, M., Kurki, J., 2012. Evaluation of a preliminary safety concept for the HPLWR, Progress in Nuclear Energy, Volume 55, Pages 68-77

Allison, C. M., and Hohorst, J. K., 2010, Role of RELAP/SCDAPSIM in Nuclear Safety, Hindawi Publishing Corporation, Science and Technology of Nuclear Installations, Volume 2010, Article ID 425658, 17 pages, doi:10.1155/2010/425658.

Bishop A.A., Sandberg R.O., Tong L.S., 1965, Forced convection heat transfer to water near critical temperatures and super-critical pressures. A.I.Ch.E.-I.Chem.E. Symposium Series. 1965, Vol. 2, S.77- 85.

Carver, M. B., Tahir, A., Kiteley, J. C., Banas, A. O., Rowe, D. S., and Midvidy, W. I., 1990, "Simulation of Flow and Phase Distribution in Vertical and Horizontal Bundles using the ASSERT-4 Subchannel Code," Nuclear Engineering and Design, 122: 413–424.

Chaaraoui, O., 2024, Thermal-hydraulic analyses in support to the development of an innovative reactor concept at supercritical pressure, MSc Thesis in Nuclear Engineering, Università di Pisa, Academic Year 2022-2023.

Chaaraoui, O., Pucciarelli, A., Ambrosini, W., Otic, I., Schulenberg, T., Allison, C., Fu, Z., 2024, Customising a system code for the analysis of the thermal-hydraulic behaviour of a supercritical pressure light water small modular reactor, Proceedings of the 2024 31st International Conference on Nuclear Engineering, ICONE31, August 4-8, 2024, Prague, Czech Republic, ICONE31- 135160

Chen. W. and Fang X., 2014. A new heat transfer correlation for supercritical water flowing in vertical tubes, International Journal of Heat and Mass Transfer. 2014. №78. P. 157–160.

Dittus, F.W., Boelter, L.M.K., 1930. Heat Transfer in Automobile Radiators of the Tubular Type, Publications in Engineering 2, University of California, Berkeley, pp. 443-461

Dubyk Y., Filonov V., Kovalenko O. and Filonova Y., 2022. Deteriorated heat transfer influence on the stress-strain state of SMR SCWR fuel bundles, ASME J of Nuclear Rad Sci. Jul 2022. Volume 8(Issue 3): 031105 (8 pages) URL: https://doi.org/10.1115/1.4052590

Dyadyakin, B.V., Popov, A.S., 1977. Heat Transfer and Thermal Resistance of Tight Seven-Rod Bundle, Cooled With Water Flow at Supercritical Pressures, Trudy VTI, 11, pp. 244–253 (in Russian)

Filonov V., Filonova Y., Dubyk Y. and Pis'mennyi E., 2022. Transfer matrix method for analysis of thermohydraulic Characteristics of supercritical water using channel Approach. International Journal of Heat and Mass Transfer. Volume 187, 15 May 2022. 122531

White, F.M. Editor. 2011. Fluid Mechanics. McGraw-Hill Series in Mechanical Engineering. McGraw Hill.

Groeneveld, D. C. and Leung, K.L. 1997. "Compendium of thermalhydraulic correlations and fluid properties (Version 1991, Rev 2), CANDU Owners Group Report No. COG-90-86

Hänninen, M., 2009. Phenomenological extensions to APROS six-equation model, VTT PUBLICATIONS 720, https://publications.vtt.fi/pdf/publications/2009/P720.pdf.

He S., He K. and Seddighi M., 2016. Laminarisation of flow at low Reynolds number due to stream wise body force, J. Fluid Mech. 2016. №809. P. 31–71.

Hussam A., Zahlan M., Laurence K. H. Leung, Yan-Ping Huang and Guang-Xu Liu, 2018. Assessment of Convective Heat Transfer Correlations Against an Expanded Database for Different Fluids at Supercritical Pressures, Journal of Nuclear Engineering and Radiation Science. 2018. №4. P. 1–14.

IAEA, 2014, Heat Transfer Behaviour and Thermohydraulics Code Testing for Supercritical Water Cooled Reactors (SCWRs); IAEA-TECDOC-1746; IAEA: Vienna, Austria, 2014.

IAEA, 2020, Understanding and Prediction of Thermohydraulic Phenomena Relevant to Supercritical Water Cooled Reactors (SCWRs); IAEA-TECDOC-1900; IAEA: Vienna, Austria, 2020.

I.E. Idelchilk, "Handbook of Hydraulic Resistance," 3rd Edition, CRC Press, 1994.

Ishiwatari, Y., Oka, Y., Koshizuka, S., Yamaji, A., Liu, J., 2005a. Safety of super LWR, (I)– safety system design. J. Nucl. Sci. Technol. 42, 927–934.

Ishiwatari, Y., Oka, Y., Koshizuka, S., Yamaji, A., Liu, J., 2005b. Safety of super LWR, (II) – safety analysis at supercritical pressure. J. Nucl. Sci. Technol. 42, 935–948.

Ivan Otic (KIT), Thomas Schulenberg (KIT), Walter Ambrosini (UNIPI), Andrea Pucciarelli (UNIPI), Omar Chaaraoui (UNIPI), Tamás Varju (BME), Attila Kiss (BME), Boglárka Babcsány (BME), Csenge Antók (BME), Péter Mészáros (BME), Zeno Bertesina (BME), Szabolcs Czifrus (BME), Vladislav Filonov (IPP), Dmitriy Fedorov (IPP), Yuliia Filonova (IPP), Yaroslav Dubyk (IPP), Armando Nava-Dominguez (CNL), Xuebin Zhao (NPIC), 2024, D3.3 Report on the preconceptual studies on the core layout and passive safety concept of the SCW-SMR, ECC-SMART Project, Deliverable D3.3.

Otic, I., et al., 2024a, D3.5 Report on CFD modelling and simulations in corroded environment under supercritical conditions, ECC-SMART Project, Deliverable D3.5.

Jackson, J., Hall, W., 1979. Forced convection heat transfer to fluids at supercritical pressure, Turbulent forced convection in channels and bundles, Vol 2, edited by S. Kakaç and D. Spalding

Jäger W., Hugo V., Espinoza S. and Hurtado A., 2011. Review and proposal for heat transfer predictions at supercritical water conditions using existing correlations and experiments, Nucl. Eng. Des., vol. 241, no. 6, pp. 2184-2203, 2011. DOI: 10.1016/j.nucengdes.2011.03.022

Kassem, S., Pucciarelli, A., and Ambrosini, W., 2022, Analysis of existing correlations for heat transfer to supercritical pressure fluids in support to the ECC-SMART Project, Università di Pisa, Dipartimento di Ingegneria Civile e Industriale, Pisa, February 11th, 2022, RL 282(2021).

Kiss Attila, Churkin Andrey, Darwan S. Pilkhwal et al., 2017. Summary on the results of two CFD benchmarks of tube and different channel geometries, Journal of Nuclear Engineering and Radiation Science, Vol. 4, №. 1. P. 1–15.

Kurganov V.A., Maslakova I.V., 2016. Normal and deteriorated heat transfer upon heating of turbulent flows of heat carriers with variable physical properties in tubes, High Temperature. 54 Iss. 4, pp.577-598

Kurganov V.A., Kaptil'nyi A.G., 1993. Flow structure and turbulent transport of a supercritical pressure fluid in a vertical tube under the conditions of mixed convection. Experimental data, Int. J. Heat Mass Transfer. Vol 36. 1993. P. 3383-3392.

Kurki, J., 2008. Simulation of thermal hydraulic at supercritical pressures with APROS. IYNC 2008. Interlaken, Switzerland, 20–26 September 2008, paper no. 145.

Kurki, J., Seppälä, M., 2009. Thermal Hydraulic Transient Analysis of the High Performance Light Water Reactor Using APROS and SMABRE, 20th International Conference on Structural Mechanics in Reactor Technology (SMiRT 20), August 9-14, 2009

Li, Y., Lu, D., Liu, Y., Zeng, X., 2014. Numerical analysis on supercritical flow instabilities using APROS, Nuclear Engineering and Design, Vol. 277, pp. 154-162

Miller, D. S., 1990, Internal Flow Systems: Design and Performance Prediction, Section 8.2., Houston, Gulf Publishing Co.

Mokry, S., Pioro, I., Kirillov, P., Gospodinov, Y., 2010. Supercritical-water heat transfer in a vertical bare tube, Nuclear Engineering and Design, Vol. 240, no. 3, pp. 568–576

Mokry, S., Pioro, I., Farah, A., King, K., Gupta, S., Peiman, W., and Kirillov, P. (2011). Development of supercritical water heat-transfer correlation for vertical bare tubes. Nucl. Eng. Des., 241(4) :1126–1136.

Nava-Dominguez, A. 2020. "Evaluation of friction-factor correlations at supercritical water conditions in support of the Canadian SCWR." J. Nucl. Eng. Radiat. Sci., 6 (3). American Society of Mechanical Engineers (ASME). https://doi.org/10.1115/1.4046783.

Pioro, I., Duffey, R., Dumouchel, T., 2004. Hydraulic resistance of fluids flowing in channels at supercritical pressures (survey), Nuclear Engineering and Design, Vol. 231, pp. 187-197

Pioro, I. L., and R. B. Duffey. 2007. Heat Transfer and Hydraulic Resistance at Supercritical Pressures in Power Engineering Applications. Power Eng. Appl. ASME Press.

Pioro, I.L., Khartabil, H.F.,2005, "Experimental Study on Heat Transfer to Supercritical Carbon Dioxide Flowing Upward in A Vertical Tube", Proc. 13th Int. Conf. on Nuc. Engg. (ICONE-13), Paper-50118, Beijing, China.

Popov V. N., 1977. Calculation of heat exchange and turbulent flow of compressible fluid in a circular tube, Teplofizika Vysokikh Temperatur, 1977, Vol. 15, No. 4, P. 795–801. (in Russian)

Razumovskiy, V., Pis' mennyy, E. N., Koloskov, A., & Pioro, I. (2008). Heat transfer to supercritical water in vertical 7-rod bundle. 48167, 963–969.

Razumovskiy, V., Pis' mennyi, E. N., Sidawi, K., Pioro, I., & Koloskov, A. E. (2016). Experimental heat transfer in an annular channel and 3-Rod bundle cooled with upward flow of supercritical water. Journal of Nuclear Engineering and Radiation Science, 2(1), 011010.

Rehme, K., 1992, "The structure of turbulence in rod bundles and the implications on natural mixing between the subchannels," International Journal of Heat and Mass Transfer, 35(2): 567–581, ISSN 0017-9310, https://doi.org/10.1016/0017-9310(92)90291-Y.

Reyman, G.A. (Ed.) 1978. A handbook of material properties for use in the analysis of light water reactor fuel rod behavior. Available on line: https://inis.iaea.org/collection/NCLCollectionStore/_Public/10/452/10452739.pdf

Rogers J.T. and Tahir A.E.E. 1975. "Turbulent Interchange Mixing on rod Bundles and the role of Secondary Flows," Heat Transfer Conference, San Francisco, Calif, USA, 1975.

SCDAP/RELAP5 Development Team, 1998, "SCDAP/RELAP5/MOD3.2 Code Manual, Vol. 1–5," NUREG/CR-6150, INEL-96/0422, July 1998.

Schlagenhaufer, M., Schulenberg, T., Starflinger, J., Bittermann, D., Andreani, M., 2010. Design proposal and parametric study of the HPLWR safety system, International Congress on Advances in Nuclear Power Plants 2010, ICAPP 2010. 1. 106-118.

SCIENTECH Inc., 1999. RELAP5/Mod3 Code Manual. Code Structure, System Models and Solution Methods, vol. I. The Thermal Hydraulics Group, Idaho.

Selander, W. N., 1978, "Explicit formulas for the computation of friction factors in turbulent pipe flow," Atomic Energy of Canada Limited Report No. AECL-6354.

Valueva E. P., 2012. Numerical modeling of heat exchange and turbulent flow of fluid within tubes at supercritical pressure, Teplofizika Vysokikh Temperatur, 2012, Vol. 50, No. 2, P. 298–306. (in Russian)

Varju, T., Csige, A., Kiss, A., Filonov, V., Filonova, Y., Fedorov, D., Pucciarelli, A., Kassem, S., Ambrosini, W., 2024. Discussion and perspectives for improvements of heat transfer correlation capabilities for fluids at supercritical pressures, Nuclear Engineering and Design, Volume 421, 113085.

Wang, H., Q. Bi, L. Wang, H. Lv, and L. K. H. Leung. 2014. "Experimental investigation of heat transfer from a 2 × 2 rod bundle to supercritical pressure water." Nucl. Eng. Des., 275: 205–218. North-Holland. https://doi.org/10.1016/J.NUCENGDES.2014.04.036.

Watts, M.J., Chou, C.T., 1982. Mixed convection heat transfer to supercritical pressure water, Int. Heat Transfer Conf. München 3, 495–500

Wheeler, C. L. et al., 1976, "COBRA-IV-I: an interim version of COBRA for thermal-hydraulic analysis of rod-bundle nuclear fuel elements and cores," Pacific Northwest National Laboratory, Battelle, WA, USA.

Xuebin Zhao (NPIC), Walter Ambrosini (UNIPI), Tamás Varju (BME), Attila Kiss (BME), Ivan Otic (KIT), Yuliia Filonova (IPP), Vladislav Filonov (IPP), Jie Zhu (UoN), 2023, Report on the results of the benchmark exercise, ECC-SMART Project, Deliverable D3.2.

Yan, L., Daogang, L., Xiaokang, Z., Yu, L., 2014. Application and evaluation of APROS to supercritical flow instability, Nuclear Power Engineering, Vol. 35(5), pp. 70-73, 88

Zhang Y., Peng M., Xia G. and Lv L., 2020. Transient thermal-hydraulic analysis of SCO2-cooled reactor system with modified RELAP5, Ann. of Nucl. Energy, vol. 147, Article 107681, 2020. DOI: 10.1016/j.anucene.2020.107681

Zhou C., Yang Y., and Cheng X., 2012. Feasibility analysis of the modified ATHLET code for supercritical water cooled systems, Nucl. Eng. Des., vol. 250, pp. 600-612, 2012. DOI: 10.1016/j.nucengdes.2012.06.021